The Astrophysical Journal, 596:663–679, 2003 October 10

A THREE-DIMENSIONAL SPHERICAL NONLINEAR INTERFACE DYNAMO

K. Zhang
School of Mathematical Sciences, University of Exeter, EX4 4QE, UK; kzhang@ex.ac.uk

K. H. Chan and J. Zou
Department of Mathematics, Chinese University of Hong Kong, Shantin, Hong Kong;
chan@math.cuhk.edu.hk, zou@math.cuhk.edu.hk

X. Liao
Shanghai Astronomical Observatory, Chinese Academy of Sciences, 80 Nandan Lu, Shanghai 200030, China;
xhliao@center.shao.ac.cn

and

G. Schubert
Department of Earth and Space Sciences and Institute of Geophysics and Planetary Physics,
UCLA, Los Angeles, CA 90095-1567; schubert@ucla.edu
Received 2003 February 24; accepted 2003 June 18

ABSTRACT

A fully three-dimensional, nonlinear, time-dependent spherical interface dynamo is investigated using a finite-element method based on the three-dimensional tetrahedralization of the spherical system. The spherical interface dynamo model consists of four zones: an electrically conducting and uniformly rotating core, a thin differentially rotating tachocline, a uniformly rotating turbulent convection envelope, and a nearly insulating exterior. The four regions are coupled magnetically through matching conditions at the interfaces. Without the effect of a tachocline, the conventional nonlinear α^2 dynamo is always stationary, axisymmetric, and equatorially antisymmetric even though numerical simulations are always fully three-dimensional and time dependent. When there is no tachocline, the azimuthal field is confined to the convection zone while the poloidal magnetic field penetrates into the radiative core. The effects of an interface dynamo with a tachocline having a purely axisymmetric toroidal velocity field are as follows: (1) the action of the steady tachocline always gives rise to an oscillatory dynamo with a period of about 2 magnetic diffusion units, or about 20 yr if the magnetic diffusivity in the convection zone is 10^8 m^2 s^{-1}; (2) the interface dynamo solution is always axisymmetric, selects dipolar symmetry, and propagates equatorward (for the assumed form of α) although the simulation is fully three-dimensional; (3) the generated magnetic field mainly concentrates in the vicinity of the interface between the tachocline and the convection zone; and (4) the strength of the toroidal magnetic field is dramatically amplified by the effect of the tachocline. Extensions of Cowling's theorem and the toroidal flow theorem to multilayer spherical shell regions with radially discontinuous magnetic diffusivities are presented.

Subject heading: Sun: magnetic fields

1. INTRODUCTION

It is widely accepted that large-scale solar magnetic activity, such as the 11 yr sunspot cycle, is the manifestation of magnetohydrodynamic processes occurring in the deep solar interior (Parker 1955; Moffatt 1978; Stix 1989). Significant progress has been made in understanding these processes through the recognition that a highly differentially rotating transition zone between the convection and radiative regions of the Sun, the solar tachocline, plays an essential role (Schou 1991; Spiegel & Zahn 1992; Parker 1993; Weiss 1994; Gough et al. 1996; Dikpati & Charbonneau 1999). It has been suggested that the solar tachocline is a strongly stably stratified layer with a thickness up to about 10% of the solar radius (Kosovichev 1996).

The solar tachocline is an ideal location for the generation and storage of the Sun's strong azimuthal magnetic fields. If the strong azimuthal fields were stored in the convection zone, they would be expelled by magnetic buoyancy on a timescale that is too short compared to the solar cycle. In other words, the large-scale solar surface magnetic activities can be interpreted as a result of the rising and emerging of tachocline-seated, strong toroidal magnetic fields driven by magnetic buoyancy (e.g., Weiss 1994). The existence of the tachocline leads naturally to the concept of the interface dynamo first proposed by Parker (1993), in which the generation of a weak poloidal magnetic field and a strong toroidal magnetic field takes place in separate fluid regions with discontinuous magnetic diffusivities across their interface. Parker's interface dynamo provides a way of generating a strong toroidal magnetic field in the vicinity of the tachocline while avoiding the dilemma of the α-quenching in the convection zone.

In Parker's Cartesian model (Parker 1993), turbulent convective motions produce an α-effect generating a weak magnetic field $\boldsymbol{B}_\alpha$ in an upper region with a large eddy magnetic diffusivity λ_α. In a lower region with a reduced magnetic diffusivity λ_ω, a uniform shear generates a strong azimuthal magnetic field $\boldsymbol{B}_\omega$. Parker showed that the linear, mean field, interface dynamo allows solutions in the form of a surface wave confined to propagate along the interface between the two fluid regions. More importantly, he demonstrated

that the ratio of the maximum magnetic field strengths on the two sides of the interface follows the scaling relation

$$\left(\frac{|\boldsymbol{B}_\omega|}{|\boldsymbol{B}_\alpha|}\right)_{\max} \sim \left(\frac{\lambda_\alpha}{\lambda_\omega}\right)^{1/2} . \quad (1)$$

When $\lambda_\alpha/\lambda_\omega \gg 1$, a strong toroidal magnetic field in the shear region can be generated by a weak magnetic field in the turbulent convection region.

There have been a number of important extensions, with different emphases, of Parker's interface dynamo model. One extension focuses on further understanding the fundamental generation mechanism of interface dynamos. MacGregor & Charbonneau (1997) considered a different interface dynamo in which the shear flow and α-effects are spatially localized in the form of delta functions on either side of the interface. Because the shear flow and α-effects are spatially separated, the effect of magnetic diffusion plays a more important role compared to the model with a uniformly distributed shear and α. By introducing the action of the Lorentz force using the Malkus-Proctor mechanism, Tobias (1997) investigated the nonlinear modulation of Parker's interface dynamo, demonstrating that the generated magnetic field can be temporally modulated. The modulated interface dynamo is capable of producing the long-term modulation of the basic solar magnetic cycle and recurrent grand minima (see also Brandenburg et al. 1989; Tobias, Weiss, & Kirk 1995; Ponty, Gilbert, & Soward 2001).

Parker's Cartesian interface dynamo has also been extended to spherical geometry (e.g., Charbonneau & MacGregor 1997; Markiel & Thomas 1999; Dikpati & Charbonneau 1999). Spherical interface dynamos usually employ a solar-like internal differential rotation profile from the helioseismic inversion (e.g., Brown et al. 1989; Schou et al. 1998),

$$\Omega(r,\theta) = \begin{cases} 0 , & 0 < r \le r_i , \\ F(r)G(\theta) , & r_i < r \le r_t , \\ G(\theta) , & r_t < r \le r_o , \end{cases} \quad (2)$$

where $\Omega(r,\theta)$ represents the differential rotation, (r, θ, ϕ) are spherical polar coordinates with $\theta = 0$ at the axis of rotation, and r_i, r_t, r_o denote the radii of the inner core, the interface between the convection zone and the tachocline, and the outer surface of the convection zone, respectively. It is important that

$$\left|\frac{dF}{dr}\right| \gg \left|\frac{1}{r}\frac{dG}{d\theta}\right| .$$

As far as magnetic field generation is concerned, the radial shear $F(r)$ in the tachocline plays a much more significant role than the latitudinal variation $G(\theta)$. In a linear spherical interface dynamo model, Charbonneau & MacGregor (1997) found a class of dynamo solutions that rely on the latitudinal shear $G(\theta)$ and that are distinct from the usual interface modes controlled by the radial shear $F(r)$. However, Markiel & Thomas (1999) showed that this class of dynamo solutions is invalid and results from an incorrect magnetic field boundary condition imposed at the interface between the core and the tachocline. The result of Markiel & Thomas (1999) demonstrated that the magnetic boundary condition can play a critical role in determining the key features of an interface dynamo and that the radial shear in the tachocline dominates the process of magnetic field generation even though latitudinal shear is present.

The primary aim of the present paper is to provide an improved understanding of the magnetic field generation process in a spherical interface dynamo through three-dimensional finite-element simulations. Following the basic interface dynamo concept of Parker (1993; see also MacGregor & Charbonneau 1997), our interface dynamo model assumes a separation between the α-effect and shear flow regions: the convectional α is nonzero only in the convection zone, while the differential rotation only occurs in the tachocline. There are two major reasons why we neglect the weaker pole-equator differential rotation in the convection zone. First, as suggested by many existing models, the weak latitudinal shear $G(\theta)$ in the convection zone is unlikely to play a dominant role in the dynamo action. More significantly, by separating the two induction sources spatially, we can isolate and identify the effect of a strong shear flow by switching on or off the action of the tachocline and hence provide insight into the interface generation mechanism.

There are a number of new features in our interface dynamo model in comparison to existing spherical models. All existing interface dynamo models are axisymmetric. The significance of nonaxisymmetric magnetic fields in mean field dynamo modeling has not been fully explored (Moss & Brandenburg 1995). This paper presents the first fully three-dimensional interface dynamo using a finite-element method in which neither spatial nor temporal symmetries are imposed. It is also the first magnetically coupled four-zone interface dynamo model. For mathematical and numerical convenience, many interface dynamo models assume the perfectly electrically conducting condition at the interface between the radiative zone and the tachocline. This assumption magnetically decouples the radiative zone from the tachocline and introduces a possible current sheet at the interface. The critical importance of the magnetic coupling between the tachocline and core was carefully demonstrated by Gough & McIntyre (1998). Moreover, the assumption of a highly stably stratified shear tachocline with a reduced magnetic diffusivity leads to $\lambda_t/\lambda_o \ll 1$ (Parker 1993), where λ_t and λ_o are magnetic diffusivities for the tachocline and the convection zone, respectively. This assumption implies a moderate magnetic diffusivity ratio, λ_i/λ_t, between the tachocline and the radiative zone, where λ_i is the magnetic diffusivity of the radiative zone. An approximation for a perfectly electrically conducting condition at the interface requires $\lambda_i/\lambda_t \to 0$, not $\lambda_i/\lambda_o \to 0$. It follows that the magnetic boundary condition at the interface may not be assumed to be perfectly conducting although the magnetic diffusivity λ_i in the radiative zone is indeed much smaller than that in the convection zone. By assuming a moderate ratio λ_i/λ_t, which requires solutions of the induction equation in the radiative zone, our model couples all the zones of the interface dynamo magnetically. It is also becoming increasingly recognized that global instabilities of the strong shear flows would lead to a nonaxisymmetric flow in the tachocline (e.g., Gilman & Fox 1997; Cally 2001; Ponty et al. 2001; Dikpati & Gilman 2001a, 2001b). This paper is the first study of the nonlinear interface dynamo driven by a nonaxisymmetric tachocline.

The remainder of the paper is organized as follows. After discussing the mathematical formulation of the problem for the interface dynamo model in § 2, we present the

finite-element formulation of the model in § 3. The results of our three-dimensional simulation are discussed in § 4. In § 5 we close the paper with a summary and some remarks.

2. MATHEMATICAL FORMULATION

The spherical interface dynamo model consists of four different zones as illustrated in Figure 1. The inner radiative sphere, $0 < r < r_i$, with constant magnetic diffusivity λ_i, rotates uniformly with the angular velocity $\boldsymbol{\Omega}_i$. If we assume a reference frame that rotates with $\boldsymbol{\Omega}_i$, the magnetic field $\boldsymbol{B}_i$ in the radiative core is governed by the equations

$$\frac{\partial \boldsymbol{B}_i}{\partial t} + \lambda_i \boldsymbol{\nabla} \times \boldsymbol{\nabla} \times \boldsymbol{B}_i = 0 \,, \tag{3}$$

$$\boldsymbol{\nabla} \cdot \boldsymbol{B}_i = 0 \,. \tag{4}$$

The magnetic field $\boldsymbol{B}_i$ cannot be generated in this uniformly rotating sphere. Above the radiative core is the tachocline, a region of strong differential rotation, $\boldsymbol{\Omega}_0 \Omega_t$, where $\boldsymbol{\Omega}_0$ is in the same direction as $\boldsymbol{\Omega}_i$, $|\boldsymbol{\Omega}_0|$ is the amplitude of the differential rotation, and Ω_t is the dimensionless profile. In the tachocline $r_i < r < r_t$, the differential rotation shears the weak poloidal magnetic field, which is generated in the convection zone and penetrates into the tachocline. The result is a strong magnetic field $\boldsymbol{B}_t$ in the tachocline. This amplification process is described by the equations

$$\frac{\partial \boldsymbol{B}_t}{\partial t} = \boldsymbol{\nabla} \times (\boldsymbol{u} \times \boldsymbol{B}_t) - \lambda_t \boldsymbol{\nabla} \times \boldsymbol{\nabla} \times \boldsymbol{B}_t \,, \tag{5}$$

$$\boldsymbol{\nabla} \cdot \boldsymbol{B}_t = 0 \,, \tag{6}$$

where $\boldsymbol{u} = (\boldsymbol{\Omega}_0 \Omega_t) \times \boldsymbol{r}$ and λ_t is the magnetic diffusivity in the tachocline. We assume a fully turbulent convection zone

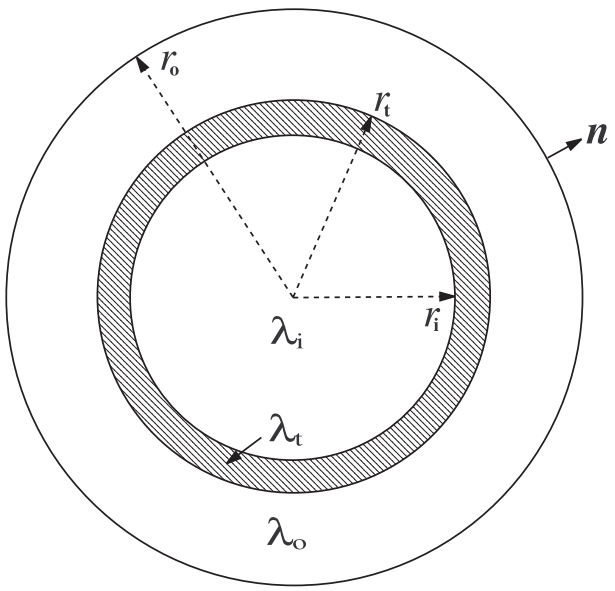

FIG. 1.—Geometry of the three-dimensional, four-zone, interface dynamo model: $0 < r \leq r_i$, the uniformly rotating, electrically conducting core with magnetic diffusivity λ_i; $r_i \leq r \leq r_t$, the differentially rotating tachocline with magnetic diffusivity λ_t; $r_t \leq r \leq r_0$, the uniformly rotating convection zone with magnetic diffusivity λ_o; and $r > r_0$, the exterior with large magnetic diffusivity λ_e. Here $\boldsymbol{n}$ is the unit normal vector.

in the region $r_t < r < r_o$. We also assume that the convection zone rotates uniformly with angular velocity $\boldsymbol{\Omega}_i$. In this zone with eddy magnetic diffusivity λ_o, where $\lambda_t/\lambda_o \ll 1$, a weak magnetic field $\boldsymbol{B}_o$ is generated by an α-effect. The nonlinear α^2 dynamo in the convection zone is described by

$$\frac{\partial \boldsymbol{B}_o}{\partial t} = \alpha_o \boldsymbol{\nabla} \times \left[\alpha \left(r, \theta, \phi, \left| \frac{\boldsymbol{B}_o}{B_{\rm eq}} \right|^2 \right) \boldsymbol{B}_o \right] - \lambda_o \boldsymbol{\nabla} \times \boldsymbol{\nabla} \times \boldsymbol{B}_o \,, \tag{7}$$

$$\boldsymbol{\nabla} \cdot \boldsymbol{B}_o = 0 \,, \tag{8}$$

where α_o is a positive parameter, $B_{\rm eq}$ is the equipartition magnetic field in the convection zone, and the three-dimensional nonlinear function $\alpha(r, \theta, \phi, |\boldsymbol{B}_o/B_{\rm eq}|^2)$ is related to the local α-quenching, as will be discussed later.

The exterior to the convection zone, $r_o < r \leq r_m$, is assumed to be nearly electrically insulating with magnetic diffusivity λ_e and rotating uniformly with angular velocity $\boldsymbol{\Omega}_i$. Its magnetic field $\boldsymbol{B}_e$ is governed by

$$\frac{\partial \boldsymbol{B}_e}{\partial t} + \lambda_e \boldsymbol{\nabla} \times (\boldsymbol{\nabla} \times \boldsymbol{B}_e) = 0 \,, \tag{9}$$

$$\boldsymbol{\nabla} \cdot \boldsymbol{B}_e = 0 \,. \tag{10}$$

For sufficiently large magnetic diffusivity λ_e such that

$$\frac{\lambda_e}{\lambda_0} \gg 1 \,,$$

the magnetic field $\boldsymbol{B}_e$ in the exterior represents an approximate potential field that is also part of the numerical dynamo solution.

We nondimensionalize length by the thickness of the convection zone $d = (r_o - r_t)$, magnetic field by the equipartition field $B_{\rm eq}$, and time by the magnetic diffusion time $\tau_m = d^2/\lambda_o$ of the convection zone. The resulting four sets of dimensionless equations for the four zones (all variables in the rest of the paper are nondimensional) are

$$\frac{\partial \boldsymbol{B}_i}{\partial t} = -\beta_i \boldsymbol{\nabla} \times \boldsymbol{\nabla} \times \boldsymbol{B}_i \,, \quad 0 < r < r_i \,, \tag{11}$$

$$\boldsymbol{\nabla} \cdot \boldsymbol{B}_i = 0 \,, \quad 0 < r < r_i \,, \tag{12}$$

$$\frac{\partial \boldsymbol{B}_t}{\partial t} = R_m \boldsymbol{\nabla} \times (\boldsymbol{u} \times \boldsymbol{B}_t) - \beta_t \boldsymbol{\nabla} \times \boldsymbol{\nabla} \times \boldsymbol{B}_t \,, \quad r_i < r < r_t \,, \tag{13}$$

$$\boldsymbol{\nabla} \cdot \boldsymbol{B}_t = 0 \,, \quad r_i < r < r_t \,, \tag{14}$$

$$\frac{\partial \boldsymbol{B}_o}{\partial t} = R_\alpha \boldsymbol{\nabla} \times \left[\alpha(r, \theta, \phi, |\boldsymbol{B}_o|^2) \boldsymbol{B}_o \right] - \boldsymbol{\nabla} \times \boldsymbol{\nabla} \times \boldsymbol{B}_o \,, \quad r_t < r < r_o \,, \tag{15}$$

$$\boldsymbol{\nabla} \cdot \boldsymbol{B}_o = 0 \,, \quad r_t < r < r_o \,, \tag{16}$$

$$\frac{\partial \boldsymbol{B}_e}{\partial t} = -\beta_m \boldsymbol{\nabla} \times \boldsymbol{\nabla} \times \boldsymbol{B}_e \,, \quad r_o < r \leq r_m \,, \tag{17}$$

$$\boldsymbol{\nabla} \cdot \boldsymbol{B}_e = 0 \,, \quad r_o < r \leq r_m \,. \tag{18}$$

There are five nondimensional quantities that characterize the interface dynamo model: the magnetic diffusivity ratios β_i, β_t, β_m, the magnetic α Reynolds number R_α, and the

magnetic ω Reynolds number R_m, which are defined by

$$\beta_i = \frac{\lambda_i}{\lambda} , \quad \beta_t = \frac{\lambda_t}{\lambda} , \quad \beta_m = \frac{\lambda_e}{\lambda_o} ,$$

$$R_\alpha = \frac{d\alpha_0}{\lambda_o} , \quad R_m = \frac{d^2|\boldsymbol{\Omega}_0|}{\lambda_o} .$$

The governing equations are solved subject to a number of matching and boundary conditions at the interfaces. At the three interfaces of the four zones, $r = r_i$, r_t, and r_0, all components of the magnetic field and the tangential component of the electrical field are continuous. These conditions yield

$$\begin{aligned}
&(\boldsymbol{B}_i - \boldsymbol{B}_t) = 0 \quad \text{at } r = r_i ,\\
&\boldsymbol{r} \times [\beta_i \nabla \times \boldsymbol{B}_i + R_m(\boldsymbol{u} \times \boldsymbol{B}_t) - \beta_t \nabla \times \boldsymbol{B}_t] = 0 \quad \text{at } r = r_i ,\\
&(\boldsymbol{B}_t - \boldsymbol{B}_o) = 0 \quad \text{at } r = r_t ,\\
&\boldsymbol{r} \times [R_m(\boldsymbol{u} \times \boldsymbol{B}_t) - \beta_t \nabla \times \boldsymbol{B}_t - R_\alpha \alpha \boldsymbol{B}_o + \nabla \times \boldsymbol{B}_o] = 0\\
&\qquad\qquad \text{at } r = r_t ,\\
&(\boldsymbol{B}_e - \boldsymbol{B}_o) = 0 \quad \text{at } r = r_o ,\\
&\boldsymbol{r} \times (\beta_m \nabla \times \boldsymbol{B}_e + R_\alpha \alpha \boldsymbol{B}_o - \nabla \times \boldsymbol{B}_o) = 0 \quad \text{at } r = r_o , \qquad (19)
\end{aligned}$$

where $\boldsymbol{r}$ is the position vector. For the boundary condition at the outer bounding surface of the dynamo solution domain, $r = r_m$, an approximation must be made. Since there are no sources at infinity, i.e.,

$$\boldsymbol{B}_e = O\left(r^{-3}\right) \quad \text{as } r \to \infty , \qquad (20)$$

we can approximate the magnetic field boundary condition at $r = r_m$ as

$$\boldsymbol{B}_e = 0 \quad \text{at } r = r_m \text{ with } \left(\frac{r_m}{r_o}\right)^3 \gg 1 . \qquad (21)$$

Equations (11)–(18), together with the matching and boundary conditions given by equations (19) and (21), define a nonlinear spherical interface dynamo problem. For given parameters of the model such as R_α and R_m, numerical solutions of the nonlinear interface dynamo are sought using a fully three-dimensional finite-element method.

In the system given by equations (11)–(18) it is the strong toroidal flow ($R_m \gg 1$) in the tachocline that dominates the process of magnetic field generation. However, it should be pointed out that dynamo action cannot occur in the first place without the α-effect in the convection zone regardless of the amplitude of the toroidal flow. An extension of the toroidal flow theorem (Bullard & Gellman 1954) to the solar context characterized by radially discontinuous magnetic diffusivities in multilayer spherical geometry is given in Appendix A. We also extend Cowling's theorem (Cowling 1934) in a sphere to the multilayer spherical system in Appendix B.

3. FINITE-ELEMENT FORMULATION

There are two major different numerical approaches for solving a dynamo problem in spherical geometry. The first one, which is widely employed in the spectral method, is the poloidal and toroidal decomposition of a magnetic field so that the solenoidal condition such as equation (14) is automatically satisfied (for example, Glatzmaier & Gilman 1982; Zhang & Busse 1989). This decomposition increases the second-order induction equation to a fourth-order equation requiring higher order shape functions when a finite-element method is employed. This usually results in inefficiency and complexity for a finite-element method. The second approach, used in this paper, is to adopt primitive variables for the magnetic field and solve both the dynamo equation and the solenoidal condition. In this case, the dynamo problem represents an overdetermined mathematical problem. This is because we have only three unknowns (B_r, B_θ, B_ϕ) but four equations in each zone.

We need to construct a mathematically equivalent dynamo problem that is not overdetermined. This can be achieved by introducing an auxiliary pressure into the dynamo equation. The finite-element formulation of our dynamo model is then given by the following four sets of modified equations: In the radiative zone,

$$\frac{\partial \boldsymbol{B}_i}{\partial t} = -\beta_i \nabla \times \nabla \times \boldsymbol{B}_i + \nabla p_i , \quad 0 < r < r_i , \qquad (22)$$

$$\nabla \cdot \boldsymbol{B}_i = 0 , \quad 0 < r < r_i , \qquad (23)$$

where the auxiliary pressure p_i is the fourth variable needed for the closure of the problem. In the tachocline,

$$\frac{\partial \boldsymbol{B}_t}{\partial t} = R_m \nabla \times (\boldsymbol{u} \times \boldsymbol{B}_t) - \beta_t \nabla \times \nabla \times \boldsymbol{B}_t + \nabla p_t , \quad r_i < r < r_t , \qquad (24)$$

$$\nabla \cdot \boldsymbol{B}_t = 0 , \quad r_i < r < r_t . \qquad (25)$$

In the convection zone,

$$\frac{\partial \boldsymbol{B}_o}{\partial t} = R_\alpha \nabla \times \left[\alpha(r, \theta, \phi, |\boldsymbol{B}_o|^2)\boldsymbol{B}_o\right] - \nabla \times \nabla \times \boldsymbol{B}_o + \nabla p_o , \quad r_i < r \le r_o , \qquad (26)$$

$$\nabla \cdot \boldsymbol{B}_o = 0 , \quad r_i < r < r_o . \qquad (27)$$

In the exterior region,

$$\frac{\partial \boldsymbol{B}_e}{\partial t} = -\beta_m \nabla \times \nabla \times \boldsymbol{B}_e + \nabla p_e , \quad r_o < r \le r_m , \qquad (28)$$

$$\nabla \cdot \boldsymbol{B}_e = 0 , \quad r_o < r \le r_m . \qquad (29)$$

The conditions that the auxiliary pressures must be continuous at the interfaces yield

$$\begin{aligned}
&p_i = p_t \quad \text{at } r = r_i ,\\
&p_t = p_o \quad \text{at } r = r_t ,\\
&p_o = p_e \quad \text{at } r = r_o . \qquad (30)
\end{aligned}$$

On the outer spherical surface $r = r_m$, we impose

$$p_e = 0 \quad \text{at } r = r_m . \qquad (31)$$

Therefore, the auxiliary pressures are analytically exactly zero or numerically very small everywhere. It follows that the dynamo problem defined by equations (11)–(18) is mathematically equivalent to that defined by equations (22)–(29). The physical pressure in the Navier-Stokes equation and the auxiliary pressure used here in the dynamo equation are fundamentally different.

Ideally, we should take the ratio (r_m/r_o) as large as possible. However, it was shown that the numerical dynamo

solutions are not significantly affected when $(r_m/r_o)^3 \geq O(10)$ (Chan et al. 2001). Practically, we take

$$\left(\frac{r_m}{r_o}\right)^3 = 27$$

throughout the paper, which gives a reasonably accurate approximation to $(r_m/r_o)^3 \rightarrow \infty$. For the ratios of magnetic diffusivities in the different zones, we use

$$\beta_m = 200\ , \quad 0.01 < \beta_i \leq 0.1\ , \quad 0.01 < \beta_t \leq 0.1$$

in our simulations.

The weak formulation for the interface dynamo using a finite-element approximation is defined by the following four sets of equations: In the radiative zone,

$$\frac{\partial}{\partial t}\int_{V_i} \boldsymbol{W}_i \cdot \boldsymbol{B}_i\, dV = -\int_{V_i} (\beta_i \boldsymbol{\nabla}\times\boldsymbol{B}_i \cdot \boldsymbol{\nabla}\times\boldsymbol{W}_i + p_i \boldsymbol{\nabla}\cdot\boldsymbol{W}_i) dV - \int_{\partial V_i} (\beta_i \hat{\boldsymbol{r}}\times\boldsymbol{\nabla}\times\boldsymbol{B} - p_i\hat{\boldsymbol{r}})\cdot\boldsymbol{W}_i\, dS\ , \tag{32}$$

$$\int_{V_i} q_i \boldsymbol{\nabla}\cdot\boldsymbol{B}_i\, dV = 0\ , \tag{33}$$

where $\hat{\boldsymbol{r}}$ is a unit vector in the radial direction, $\boldsymbol{W}_i$ and q_i are the weighting functions, V_i denotes the domain $0 \leq r \leq r_i$, and ∂V_i denotes the interface between the radiative zone and the tachocline at $r = r_i$. In the tachocline, we have

$$\frac{\partial}{\partial t}\int_{V_t} \boldsymbol{W}_t \cdot \boldsymbol{B}_t\, dV = \int_{V_t} [(R_m \boldsymbol{u}\times\boldsymbol{B}_t - \beta_t \boldsymbol{\nabla}\times\boldsymbol{B}_t)\cdot\boldsymbol{\nabla}\times\boldsymbol{W}_t + p_t\boldsymbol{\nabla}\cdot\boldsymbol{W}_t] dV + \int_{\partial V_t} [R_m\hat{\boldsymbol{r}}\times(\boldsymbol{u}\times\boldsymbol{B}_t) + \beta_t\hat{\boldsymbol{r}}\times\boldsymbol{\nabla}\times\boldsymbol{B}_t + p_t\hat{\boldsymbol{r}}]\cdot\boldsymbol{W}_t\, dS - \int_{\partial V_i} [R_m\hat{\boldsymbol{r}}\times(\boldsymbol{u}\times\boldsymbol{B}_t) + \beta_t\hat{\boldsymbol{r}}\times\boldsymbol{\nabla}\times\boldsymbol{B}_t + p_t\hat{\boldsymbol{r}}]\cdot\boldsymbol{W}_t\, dS\ , \tag{34}$$

$$\int_{V_t} q_t \boldsymbol{\nabla}\cdot\boldsymbol{B}_t\, dV = 0\ , \tag{35}$$

where $\boldsymbol{W}_t$ and q_t are the weighting functions, V_t denotes the domain $r_i \leq r \leq r_t$, and ∂V_t denotes the interface between the convection zone and the tachocline at $r = r_t$. In the convection zone, we obtain

$$\frac{\partial}{\partial t}\int_{V_o} \boldsymbol{W}_o \cdot \boldsymbol{B}_o\, dV = \int_{V_o} \{[R_\alpha \alpha(|\boldsymbol{B}_o|^2)\boldsymbol{B}_o - \boldsymbol{\nabla}\times\boldsymbol{B}_o]\cdot\boldsymbol{\nabla}\times\boldsymbol{W}_o + p_o\boldsymbol{\nabla}\cdot\boldsymbol{W}_o\} dV + \int_{\partial V_t} [R_\alpha\alpha(|\boldsymbol{B}_o|^2)\boldsymbol{B}_o - \hat{\boldsymbol{r}}\times\boldsymbol{\nabla}\times\boldsymbol{B}_o + p_o\hat{\boldsymbol{r}}]\cdot\boldsymbol{W}_o\, dS - \int_{\partial V_o} [R_\alpha\alpha(|\boldsymbol{B}_o|^2)\boldsymbol{B}_o - \hat{\boldsymbol{r}}\times\boldsymbol{\nabla}\times\boldsymbol{B}_o + p_o\hat{\boldsymbol{r}}]\cdot\boldsymbol{W}_o\, dS\ , \tag{36}$$

$$\int_{V_o} q_o \boldsymbol{\nabla}\cdot\boldsymbol{B}_o\, dV = 0\ , \tag{37}$$

where $\boldsymbol{W}_o$ and q_o are the weighting functions, V_o denotes the domain $r_t \leq r \leq r_o$, and ∂V_o denotes the interface between the convection zone and the exterior at $r = r_o$. In the exterior region, V_e, defined by the region $r_o \leq r \leq r_m$, we have

$$\frac{\partial}{\partial t}\int_{V_e} \boldsymbol{W}_e \cdot \boldsymbol{B}_e\, dV = \int_{V_e} (-\beta_e \boldsymbol{\nabla}\times\boldsymbol{B}_e\cdot\boldsymbol{\nabla}\times\boldsymbol{W}_e + p_e\boldsymbol{\nabla}\cdot\boldsymbol{W}_e) dV + \int_{\partial V_o} (\beta_e\hat{\boldsymbol{r}}\times\boldsymbol{\nabla}\times\boldsymbol{B}_e - p_e\hat{\boldsymbol{r}})\cdot\boldsymbol{W}_e\, dS\ , \tag{38}$$

$$\int_{V_e} q_e \boldsymbol{\nabla}\cdot\boldsymbol{B}_e\, dV = 0\ , \tag{39}$$

where $\boldsymbol{W}_e$ and q_e are the weighting functions and we have made use of the boundary conditions at $r = r_m$.

After the three-dimensional tetrahedralization of the whole spherical system, the finite-element approximation for the magnetic field and the pressure can be written as

$$\boldsymbol{B} = (\boldsymbol{B}_i, \boldsymbol{B}_t, \boldsymbol{B}_o, \boldsymbol{B}_e) = \left[\sum_j \boldsymbol{B}_i^j(t)N_j(\boldsymbol{r}), \sum_j \boldsymbol{B}_t^j(t)N_j(\boldsymbol{r}), \sum_j \boldsymbol{B}_o^j(t)N_j(\boldsymbol{r}), \sum_j \boldsymbol{B}_e^j(t)N_j(\boldsymbol{r})\right]\ , \tag{40}$$

$$p = (p_i, p_t, p_o, p_e) = \left[\sum_j p_i^j(t)M_j(\boldsymbol{r}), \sum_j p_t^j(t)M_j(\boldsymbol{r}), \sum_j p_o^j(t)M_j(\boldsymbol{r}), \sum_j p_e^j(t)M_j(\boldsymbol{r})\right]\ , \tag{41}$$

where $M_j(\boldsymbol{r})$ and $N_j(\boldsymbol{r})$ are shape functions defined in each tetrahedron element and $\boldsymbol{B}_i^j$ and p_i^j, for example, denote the value of $\boldsymbol{B}_i$ and p_i at the jth node. The shape functions $M_j(\boldsymbol{r})$ in a tetrahedron are defined by

$$M_1 = L_1\ , \quad M_2 = L_2\ , \quad M_3 = L_3\ , \quad M_4 = L_4\ , \tag{42}$$

where L_j ($j = 1, 2, 3, 4$) are the volume coordinates for a tetrahedron, and satisfy

$$M_j(\boldsymbol{r}_i) = \delta_{ij}\ , \quad \sum_{j=1}^{4} M_j(\boldsymbol{r}) = 1\ . \tag{43}$$

The shape functions $N_j(\boldsymbol{r})$ in a tetrahedron are defined by

$$\begin{aligned} N_1 &= L_1(2L_1 - 1)\ , \quad N_2 = L_2(2L_2 - 1)\ , \\ N_3 &= L_3(2L_3 - 1)\ , \quad N_4 = L_4(2L_4 - 1)\ , \\ N_5 &= 4L_1L_2\ , \quad N_6 = 4L_1L_3\ , \\ N_7 &= 4L_1L_4\ , \quad N_8 = 4L_2L_3\ , \\ N_9 &= 4L_2L_4\ , \quad N_{10} = 4L_3L_4 \end{aligned} \tag{44}$$

and satisfy

$$N_j(\boldsymbol{r}_i) = \delta_{ij} , \quad \sum_{j=1}^{10} N_j(\boldsymbol{r}) = 1 . \tag{45}$$

In other words, there are four nodes for the pressure in each tetrahedron (the four corners) and 10 nodes for the magnetic field (the four vertices and six middle points of the six edges of each tetrahedron). The weight functions are selected to be the same as the expansions used in equations (40) and (41).

After substitution of equations (40) and (41) and the corresponding weight functions into equations (32)–(39), we evaluate the integral over the spherical zone as a sum of integrals over the tetrahedron element domains. After carrying out the integration over all the tetrahedra and coupling the four zones together by the magnetic field matching conditions, we obtain a system of nonlinear ordinary differential equations. The system represents a typical saddle point problem. A Crank-Nicholson scheme is then used for time integration wherein the nonlinear term is treated explicitly by a second-order extrapolation while all the linear terms are treated explicitly. The resulting linear system is solved by an iterative method.

4. SIMULATIONS OF THE SPHERICAL INTERFACE DYNAMO

4.1. *Stationary Conventional Dynamos*

First, we switch off the interface dynamo by setting $R_m \equiv 0$ in equation (24) so that the tachocline disappears and becomes part of the uniformly rotating radiative core. In the noninterface dynamo simulation, we take

$$\begin{aligned} \boldsymbol{u}(r,\theta,\phi) &= (u_\phi, u_r, u_\theta) = (0,\ 0,\ 0) , \quad r_i < r \le r_t , \\ \alpha(r,\theta,\phi) &= \sin^2\theta\cos\theta\sin\left[\pi\frac{(r-r_t)}{(r_o-r_t)}\right]\frac{1}{(1+|\boldsymbol{B}_o|^2)} , \\ & \qquad r_t < r \le r_o , \end{aligned} \tag{46}$$

where (u_ϕ, u_r, u_θ) denote the three components of the velocity in spherical polar coordinates. The α formula assumes that the strength of the α-effect will be suppressed when the kinetic energy of the flow is comparable to the magnetic energy, which has been widely used, for example, by Choudhuri, Schüssler, & Dikpati (1995) and Küker, Rüdiger, & Schultz (2001; for a detailed discussion see Brandenburg 1994). A major advantage of this formulation is that it allows simulation of many essential physical dynamo processes without reference to the difficult dynamics of strong nonlinear interaction between the flow and the Lorentz force.

We have assumed an α-effect throughout the whole convection zone. This is physically reasonable if the α-effect is directly related to turbulent convective motions (Moffatt 1978). In some dynamo models (e.g., Charbonneau & MacGregor 1997), the α-effect is strongly concentrated near the base of the convection envelope to avoid excitation of dynamo modes associated exclusively with the latitudinal angular velocity gradient in the convection zone. This is not a concern in the present model. Since the toroidal magnetic field in our interface dynamo is generated only in the tachocline, magnetic buoyancy in the bulk of the convection zone is not an issue (Fan, Fisher, & De Luca 1993; Caligari, Moreno-Insertis, & Schussler 1995). The resulting dynamo using equation (46) corresponds to a well-understood conventional α^2 dynamo (e.g., Roberts 1972). We have tested various α distributions and found that the principal results are not critically affected by the particular choice of α. Note that the local α-quenching is the only nonlinearity in this dynamo model.

Apart from the azimuthal symmetries of a dynamo solution, there exist two different equatorial parities for the magnetic field, an equatorially symmetric dynamo with

$$(B_\phi, B_r, B_\theta)(\theta) = (B_\phi, B_r, -B_\theta)(\pi - \theta)$$

and an equatorially antisymmetric dynamo obeying

$$(B_\phi, B_r, B_\theta)(\theta) = (-B_\phi, -B_r, B_\theta)(\pi - \theta) ,$$

which is usually referred to as dipolar symmetry. Our nonlinear simulation does not impose any azimuthal or equatorial symmetries.

Our calculations show that any initial magnetic field decays with increasing time if $R_\alpha < 18$ and grows if $R_\alpha > 18$. Furthermore, the properties of the nonlinear dynamo are not dependent on initial conditions. The onset of dynamo action takes place at about $R_\alpha = 18$. Without the effect of a tachocline, the conventional nonlinear dynamo is always stationary, axisymmetric, and equatorially dipolar even though numerical simulations are always fully three-dimensional and time dependent. Four typical nonlinear stationary solutions are presented in Figure 2, showing the magnetic energy E_m of the generated magnetic field as a function of time, where

$$E_m = \int_V |\boldsymbol{B}|^2 dV$$

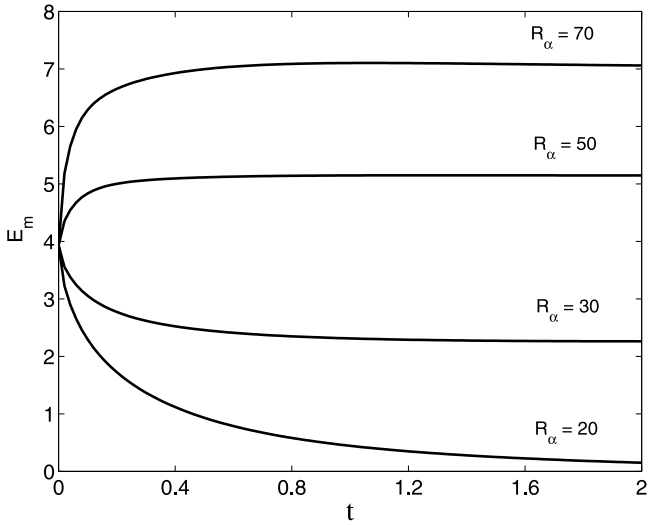

FIG. 2.—Magnetic energy E_m as a function of time for the conventional α^2 dynamo without the effect of a tachocline. Four nonlinear dynamo solutions are shown, and the onset of dynamo action occurs at about $R_\alpha \approx 18$.

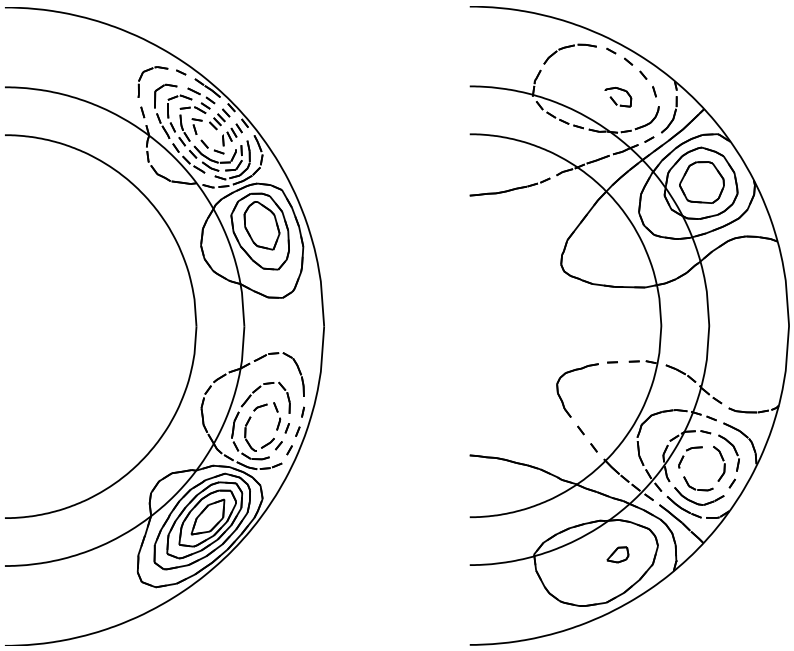

FIG. 3.—Contours of the azimuthal (radial) field B_ϕ (B_r) in a meridional plane on the left-hand (right-hand) panel for the conventional α^2 dynamo without the effect of the tachocline for $R_\alpha = 30$ with $\beta_i = \beta_t = 0.1$. Dashed contours indicate azimuthal field lines with $B_\phi < 0$ ($B_r < 0$), and solid contours correspond to fields with $B_\phi > 0$ ($B_r > 0$). The contour levels for both B_ϕ and B_r are from -0.55 to 0.55.

and V denotes the region $r_i \le r \le r_0$. The planform of the generated azimuthal field in a meridional plane for $R_\alpha = 30$ with $\beta_i = \beta_t = 0.1$ is depicted in Figure 3. The azimuthal magnetic field is largely confined to the convection zone. Its maximum dimensionless strength is about $\left|B_\phi\right|_{\max} = 0.5$. The poloidal magnetic field, which has about the same strength as that of the toroidal field, penetrates into the deep interior all the way to the radiative core. Dynamo solutions calculated with different values of β_i and β_t show qualitatively similar features.

4.2. *Interface Dynamos with Two-dimensional Tachocline*

We now switch on the interface dynamo by introducing a nonzero axisymmetric shear flow in the tachocline while keeping the same α distribution as in equation (46),

$$\begin{aligned} \boldsymbol{u}(r,\theta,\phi) &= (u_\phi, u_r, u_\theta) \\ &= \left\{ \Omega_t(\theta) r \sin\theta \sin\left[\pi \frac{(r-r_i)}{(r_t-r_i)}\right],\ 0,\ 0 \right\}, \\ & \qquad r_i < r \le r_t\ , \end{aligned} \tag{47}$$

where $\Omega_t(\theta)$ represents the three-term expression approximating the observed profile of the solar differential rotation (Schou et al. 1998),

$$\Omega_t(\theta) = 1 - 1.98\cos^2\theta - 3.26\cos^4\theta\ .$$

It is found that the principal properties of the simulated dynamo are not particularly sensitive to the choice of $\Omega_t(\theta)$. The weaker pole-equator differential rotation in the convection zone is neglected. We assume that the differential rotation vanishes at the interface $r = r_t$, which spatially separates the two magnetic induction sources (Parker 1993; MacGregor & Charbonneau 1997). This separation enables us to understand how an interface dynamo operates in multilayer spherical systems. Without the α-effect in the convection zone, dynamo action cannot be sustained by the purely toroidal axisymmetric flow in the tachocline.

The magnetic energy as a function of time is shown in Figure 4 for $R_m = 100$ and 200. The two solutions of the interface dynamo are obtained using the same parameters as in Figures 2 and 3 ($R_\alpha = 30$ with $\beta_i = \beta_t = 0.1$) except for the presence of the tachocline. Contours of the azimuthal magnetic field at the interface r_t plotted against time (which is usually referred to as the butterfly diagram) and the structure of the generated toroidal field in a meridional plane are shown in Figures 4 and 5, respectively, for $R_m = 200$ with $\beta_i = \beta_t = 0.1$. The results are robust in that many more simulations in various parameter regimes, for example, smaller values of β_i, always show qualitatively similar features.

An important insight into the interface dynamo mechanism can be obtained by comparing the interface dynamo shown in Figures 4 and 5 to the noninterface dynamo in Figures 2 and 3. The comparison reveals a number of significant effects of the tachocline: (1) the action of the steady tachocline always gives rise to an oscillatory dynamo with a period of about 2 magnetic diffusion units, $2\tau_m$, or about 20 yr if we adopt $\lambda_o = 10^8$ m^2 s^{-1}; (2) the interface dynamo solution with α given by equation (46) and Ω_t given by equation (47) is always axisymmetric, selects dipolar symmetry, and propagates equatorward although the simulation is fully three-dimensional (if the sign of α in eq. [46] changes, the corresponding dynamo wave would propagate poleward);

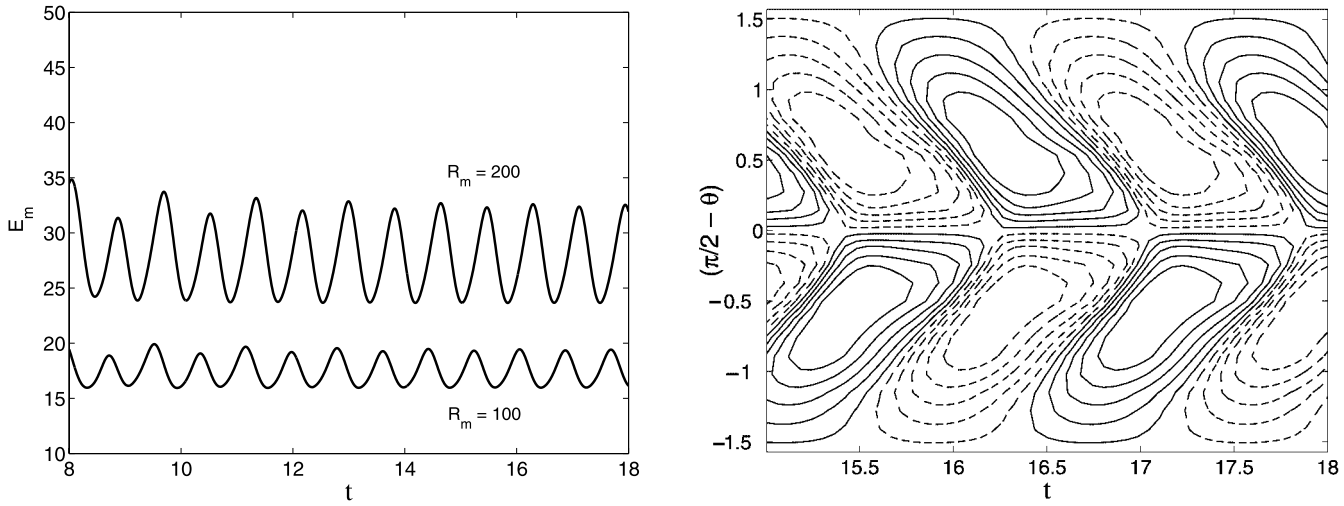

FIG. 4.—*Left:* Magnetic energy E_m as a function of time with a steady axisymmetric tachocline for $R_\alpha = 30$ with $\beta_t = \beta_i = 0.1$. *Right:* Butterfly diagram for the solution $R_m = 200$ with the azimuthal magnetic field evaluated at the interface between the tachocline and convection zone. The contour levels for B_ϕ in the butterfly diagram are from -6.5 to 6.5.

(3) the generated magnetic field mainly concentrates in the vicinity of the interface between the tachocline and the convection zone; and (4) the strength of the toroidal magnetic field is dramatically amplified by the effect of the tachocline, reaching the maximum strength $|B_\phi|_{\max} = 6$, about a factor of 10 larger than that of the corresponding noninterface dynamo. Such strong toroidal magnetic fields in the tachocline are susceptible to magnetic buoyancy instabilities leading to a quick eruption of the field onto the surface of the Sun in the form of sunspots.

It is not surprising that the action of the shear flow in the tachocline gives rise to a time-dependent dynamo. Parker (1970) argued that unsteady solutions of the α-ω dynamo should be the norm. The argument was clearly illustrated by free modes of the α-ω dynamo (Moffatt 1978). However, it is somewhat surprising that we cannot find any solutions of the time-dependent dynamo that propagate azimuthally in the three-dimensional simulations. Mathematically speaking, there exist two different types of time-dependent dynamos when both the α and shear flow are axisymmetric: one propagates equatorward or poleward and the other propagates eastward or westward. The latter is usually preferred in three-dimensional kinematic dynamos (e.g., Gubbins et al. 2000) or in convection-driven dynamic dynamos (e.g., Zhang & Busse 1989). The results of our three-dimensional simulations suggest that the axisymmetric assumption of a spherical interface dynamo with an axisymmetric tachocline is robust.

4.3. *Interface Dynamos with Three-dimensional α*

The preference for nonaxisymmetric dynamo modes is found in some conventional dynamo models where differential rotation is weak (e.g., Roberts & Stix 1972; Moss, Tuominen, & Brandenburg 1991). All our fully three-dimensional simulations using an axisymmetric α distribution have so far produced an axisymmetric magnetic field. Nonaxisymmetric mean magnetic fields can be produced by a nonaxisymmetric α distribution as studied in the conventional mean field dynamo framework (Rüdiger 1980; Moss & Brandenburg 1995). Following this idea, we consider a nonaxisymmetric interface dynamo with a nonaxisymmetric α distribution in the form

$$\alpha(r,\theta,\phi) = \sin^2\theta\cos\theta(1+\epsilon\sin m\phi) \times \sin\left[\pi\frac{(r-r_t)}{(r_o-r_t)}\right]\frac{1}{(1+|\boldsymbol{B}_o|^2)}\,, \qquad r_t < r \le r_o\,, \tag{48}$$

where $\epsilon = 0$ recovers the axisymmetric case, m is an azimuthal wavenumber, and $\boldsymbol{u}$ is the same as in equation (47).

Figure 6 shows the results of two dynamo solutions using the α distribution of equation (48) with $m = 1$ and $\epsilon = 0.5$ and 0.75. The butterfly diagram in Figure 6 is shown only for $\phi = 0$ since the butterfly diagrams plotted at different ϕ are quite similar. This is because the generation mechanism is still predominantly the shear flow in the axisymmetric tachocline. The nonaxisymmetric nonlinear interface dynamo is periodic and still propagates toward the equator with an approximate period of about $2\tau_m$. This appears to be a general feature of all our dynamo simulations, most of which are not shown here. In Figure 7 we show the contours of the radial magnetic field on the spherical surface $r = r_o$ viewed from the South Pole and the corresponding toroidal field in a meridional plane at different times. A nonaxisymmetric time-dependent dynamo wave does not have to propagate equatorward or polarward. In fact, nonaxisymmetric dynamo waves usually propagate in the azimuthal direction without the effect of a tachocline (Zhang & Busse 1989). However, the nonlinear interface dynamo wave shown in Figure 7 always propagates equatorward. In addition, there is no azimuthal propagation in this case. These characteristics reveal the essential importance of the tachocline in the magnetic field generation process for a spherical interface dynamo.

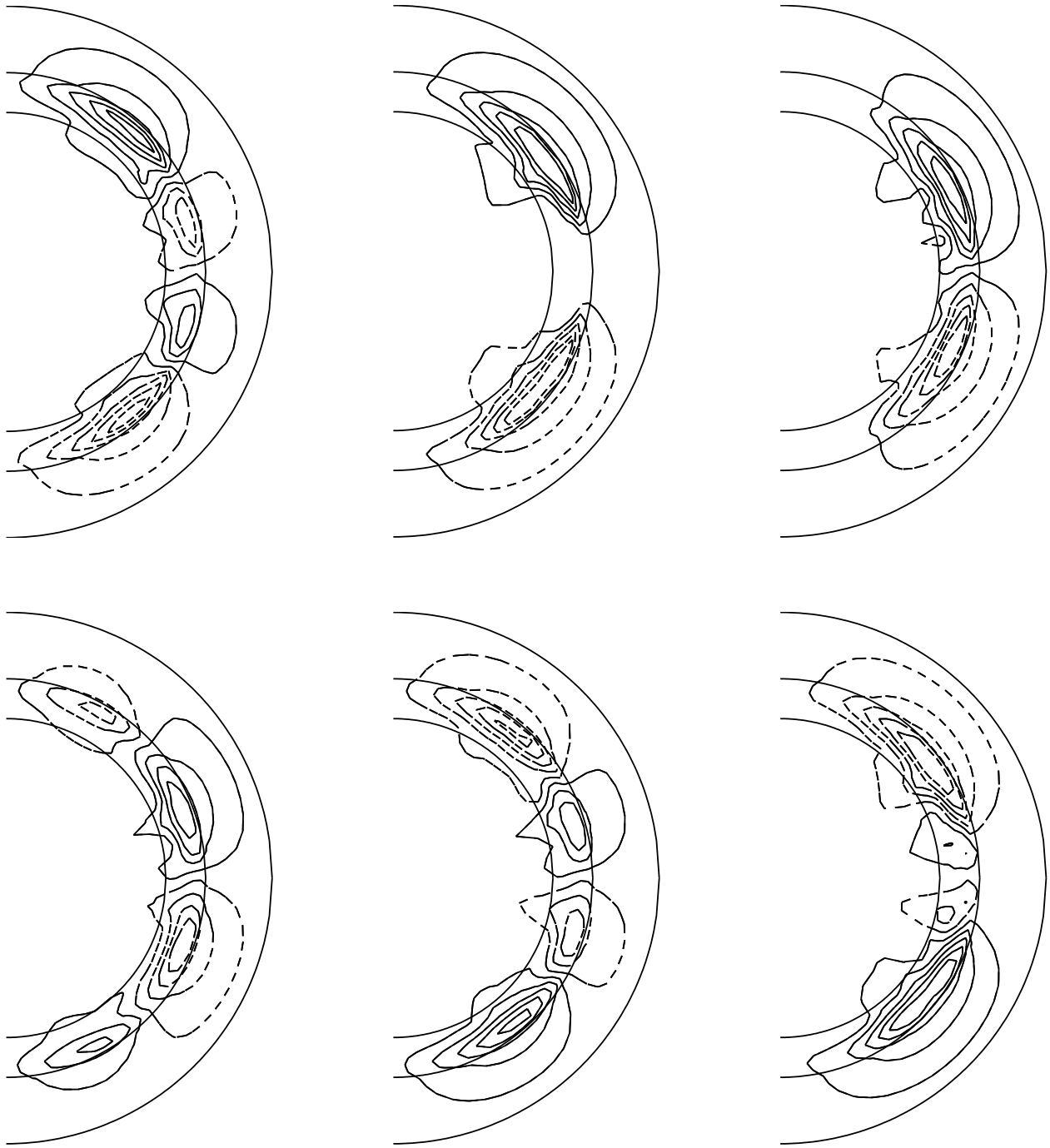

FIG. 5.—Contours of the azimuthal field B_ϕ in a meridional plane plotted at six different instants, $t = 16.0, 16.2, 16.4, 16.6, 16.8, 17.0$ (from top left to right and then from bottom left to right) for $R_m = 200$, $R_\alpha = 30$ with $\beta_t = \beta_i = 0.1$. The contour levels for B_ϕ are from -12 to 12.

4.4. *Interface Dynamos with Three-dimensional Tachocline*

Global instabilities in rotating spherical systems with a toroidal magnetic field or a differential rotation have been extensively studied. It was shown by Gilman & Fox (1997) that even very simple differential rotation can become unstable to azimuthal wavenumber $m = 1$ disturbances in the presence of a moderate magnetic field (see also Cally 2001). Using a shallow-water model, Gilman & Dikpati (2002; see also Dikpati & Gilman 2001a, 2001b) studied instabilities of the solar tachocline differential rotation, showing that the azimuthal wavenumber $m = 1$ again represents the most unstable mode. In a fully three-dimensional stability analysis for a toroidal magnetic field in rotating spherical systems, Zhang, Liao, & Schubert (2003) demonstrate analytically that the magnetohydrodynamic system is unstable to the $m = 1$ perturbation. It is therefore likely that the shear flow in the tachocline, as a result of hydrodynamic or magnetic instabilities, is not purely axisymmetric but is weakly nonaxisymmetric and characterized by the azimuthal wavenumber $m = 1$. The $m = 1$ instability would lead to nonaxisymmetric poloidal flows in the tachocline.

To examine the effect of a nonaxisymmetric flow in the tachocline, we assume a kinematically possible

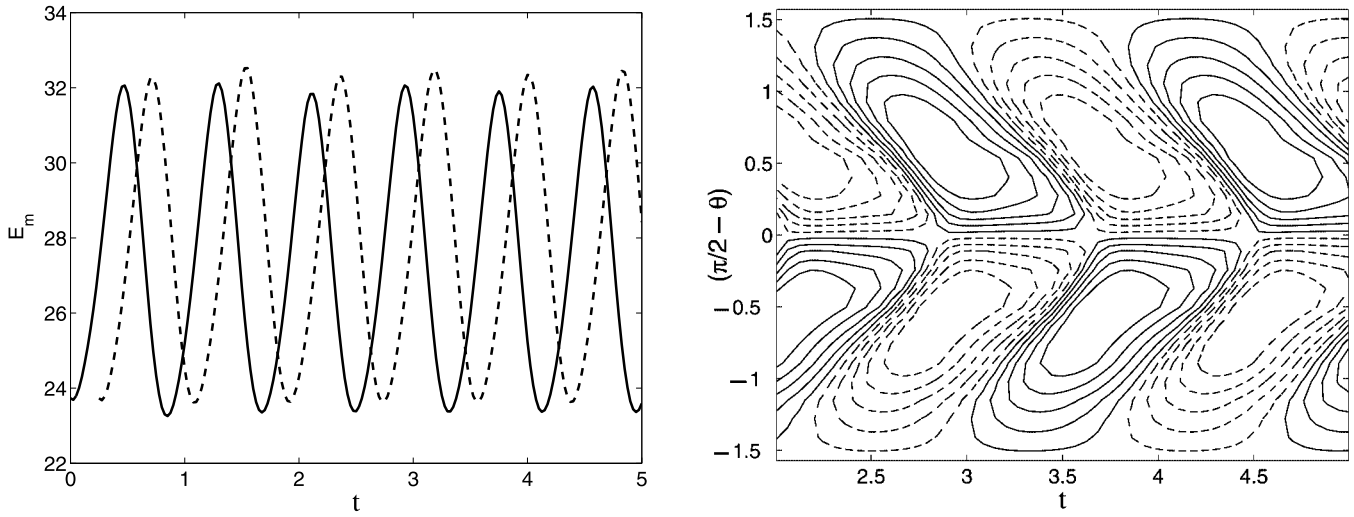

FIG. 6.—Nonaxisymmetric interface dynamos with $R_m = 200$, $R_\alpha = 30$. *Left:* Magnetic energies E_m as a function of time for $\epsilon = 0.5$ (*solid line*) and 0.75 (*dashed line*). *Right:* Butterfly diagram for the dynamo solution at $\phi = 0$ with B_ϕ evaluated at the interface between the tachocline and convection zone for $\epsilon = 0.75$. The contour levels for B_ϕ in the butterfly diagram are from −6.5 to 6.5.

three-dimensional flow satisfying the conservation of mass $\nabla \cdot \boldsymbol{u} = 0$,

$$u_\phi = \Omega_t(\theta) r \sin\theta \left\{ \sin\left[\pi \frac{(r - r_i)}{(r_t - r_i)}\right] + \frac{\epsilon_\phi \pi}{2r^2 (r_t - r_i)} \sin\left[2\pi \frac{(r - r_i)}{(r_t - r_i)}\right] \sin(m\phi) \right\}, \quad r_i < r \le r_t,$$

$$u_r = -\frac{\epsilon_\phi \Omega_t(\theta) \cos(m\phi)}{2r^2} \sin^2\left[\pi \frac{(r - r_i)}{(r_t - r_i)}\right], \quad r_i \le r \le r_t,$$

$$\alpha = \sin^2\theta \cos\theta \sin\left[\pi \frac{(r - r_t)}{(r_o - r_t)}\right] \frac{1}{(1 + |\boldsymbol{B}_o|^2)}, \quad r_t < r \le r_o, \tag{49}$$

where the parameter ϵ_ϕ provides a measure of the tachocline's departure from the axisymmetric state and $\Omega_t(\theta)$ is still given by the three-term expression below equation (47).

We have performed a number of simulations using various parameters of the model, in particular, with different values of β_i and β_t. The magnetic energy versus time for typical dynamo solutions is shown in Figure 8 for $\epsilon_\phi = 0.25$ and 0.5 for $\beta_i = \beta_t = 0.1$ with $m = 1$. The fundamental properties of the axisymmetric interface dynamo, such as the equatorward-propagating dynamo wave with a period of about $2\tau_m$, are not altered. The time-dependent structure of the nonaxisymmetric, equatorward-propagating dynamo wave is shown by the contours of B_ϕ at the spherical interface between the convection zone and the tachocline and the corresponding radial field in a meridional plane in Figure 9. The strength of the toroidal magnetic field reaches the maximum strength $|B_\phi|_{\max} = 10$, i.e., about 10^5 G if we take $B_{\rm eq} = 10^4$ G. There exists a particular longitudinal region in which the toroidal magnetic field is much stronger than in other longitudinal regions. A strong toroidal magnetic field in that particular longitudinal region would be more susceptible to magnetic buoyancy instability, leading to stronger eruption or more magnetic activity in the region. Although a nonaxisymmetric dynamo wave is allowed to propagate azimuthally in fully three-dimensional simulations, the three-dimensional dynamo wave shown in Figure 9 always propagates equatorward with α given by equation (46) and Ω_t given by equation (47).

5. SUMMARY AND REMARKS

We have investigated a fully three-dimensional, nonlinear, time-dependent, spherical interface dynamo using a finite-element method based on the three-dimensional tetrahedralization of the spherical system. The dynamo model consists of four regions, an electrically conducting uniformly rotating core, a thin differentially rotating tachocline, a uniformly rotating and electrically conducting convection envelope, and a uniformly rotating and nearly insulating exterior. The four regions are coupled magnetically through the matching conditions at the interfaces.

We have presented a small number of many dynamo simulations carried out for a broad range of parameter values. This is because the results of the nonlinear dynamo simulations presented are very robust. Nearly all our calculations using various values of R_m, R_α, β_i, and β_t (where β_i and β_t are moderately small) produce qualitatively similar dynamos having a predominantly toroidal magnetic field in the vicinity of the tachocline, an equatorward-propagating dynamo wave with a period of about 2 diffusion time units, and dipolar symmetries despite fully three-dimensional simulations.

This robustness is perhaps attributable to the global magnetic field boundary condition used at the inner core-tachocline interface. In contrast to the velocity boundary condition (which is local), the magnetic field boundary condition at the interface is global and plays a major role in controlling how the magnetic field is generated (Hollerbach & Jones 1993; Markiel & Thomas 1999; Schubert & Zhang 2000). The magnetic field $\boldsymbol{B}$ for an axisymmetric interface dynamo is usually expressed as

$$\boldsymbol{B} = B_\phi \hat{\boldsymbol{\phi}} + \nabla \times (A \hat{\boldsymbol{\phi}}), \tag{50}$$

where $\hat{\boldsymbol{\phi}}$ is a unit vector in the azimuthal direction. To obtain the mathematically convenient local boundary condition

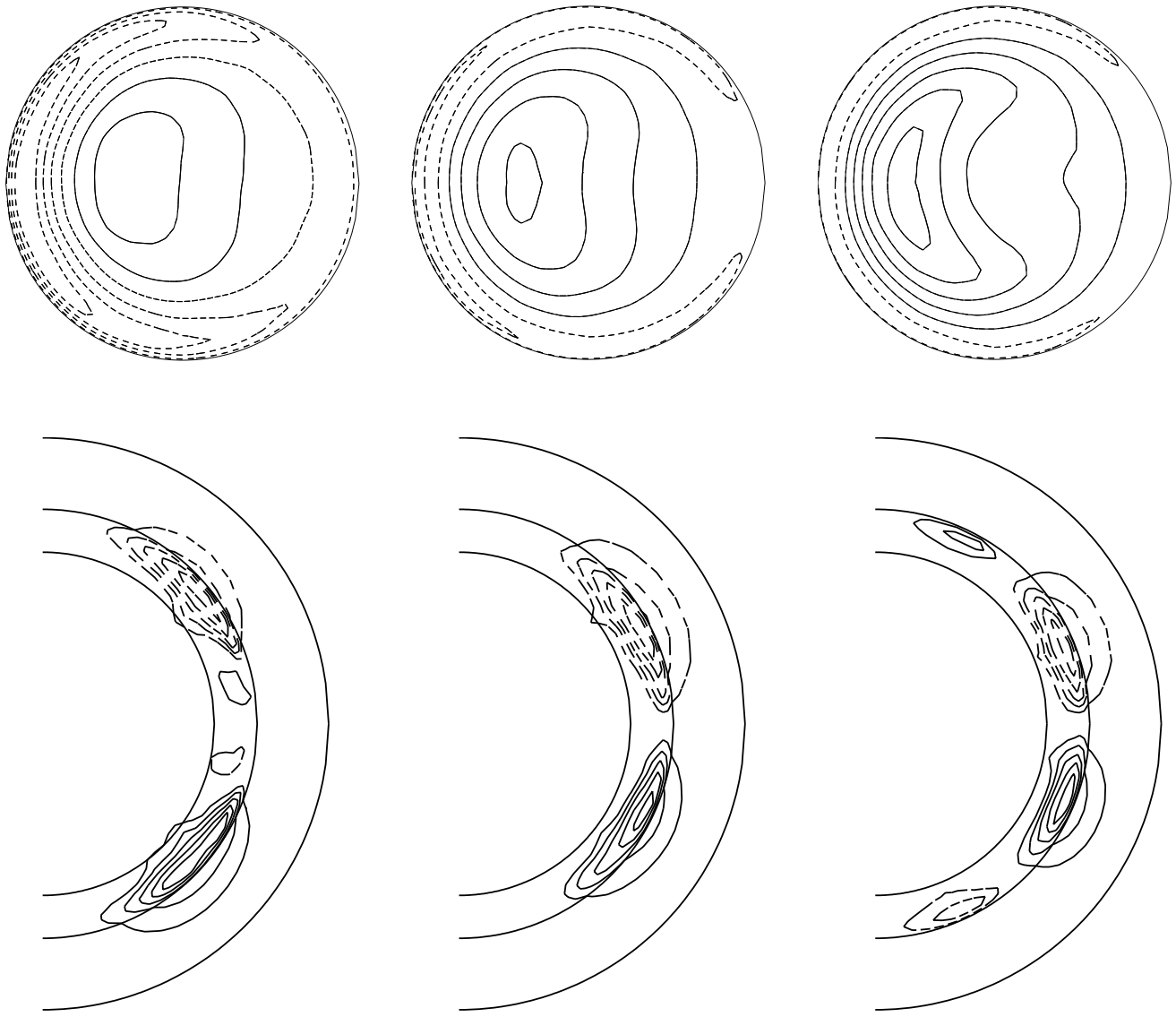

FIG. 7.—Contours of B_r at the spherical surface $r = r_0$ viewed from the South Pole (from top left to right) and contours of B_ϕ in a meridional plane $\phi = \pi$ (from bottom left to right) plotted at three different instants for $t = 3.6$, 3.8, 4.0. The parameters are $R_m = 200$ and $\beta_t = \beta_i = 0.1$. Dashed contours indicate fields with $B_r < 0$ ($B_\phi < 0$) and solid contours correspond to $B_r > 0$ ($B_\phi > 0$). The contour levels for B_ϕ (B_r) are from -12 to 12 (-0.45 to 0.45).

that decouples the radiative core completely from the dynamo operating system, some dynamo models assume that the electromagnetic boundary condition at the interface between the radiative core and tachocline is simply given by

$$B_\phi = A = 0 \quad \text{at } r = r_i \,, \tag{51}$$

which is inappropriate. The solar dynamo is perhaps characterized by $\beta_i \ll 1$, $\beta_t \ll 1$ together with $\beta_i/\beta_t \ll 1$. Our experience indicates that a direct numerical simulation for this parameter regime is rather difficult and an analytical approach is more inappropriate.

As the first step toward the construction of a realistic fully three-dimensional finite-element solar dynamo model, we have followed the idea of Parker's interface dynamo (see also Charbonneau & MacGregor 1997; Tobias 1997) by separating the α- and ω-processes spatially. There are several important ingredients in the real solar dynamo that are not present in our model. One of them is the differential rotation and meridional circulation in the convection zone. A large-scale

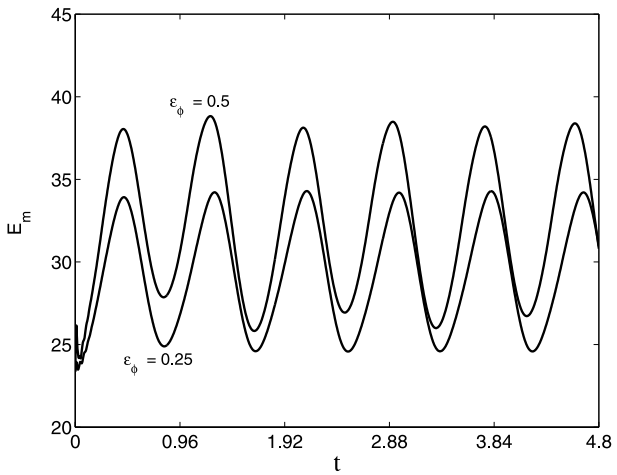

FIG. 8.—Two interface dynamo solutions obtained with the nonaxisymmetric tachocline with $m = 1$ for $R_m = 200$, $R_\alpha = 30$, showing the magnetic energy E_m as a function of time for $\epsilon_\phi = 0.25$ and 0.5 with $\beta_t = \beta_i = 0.1$.

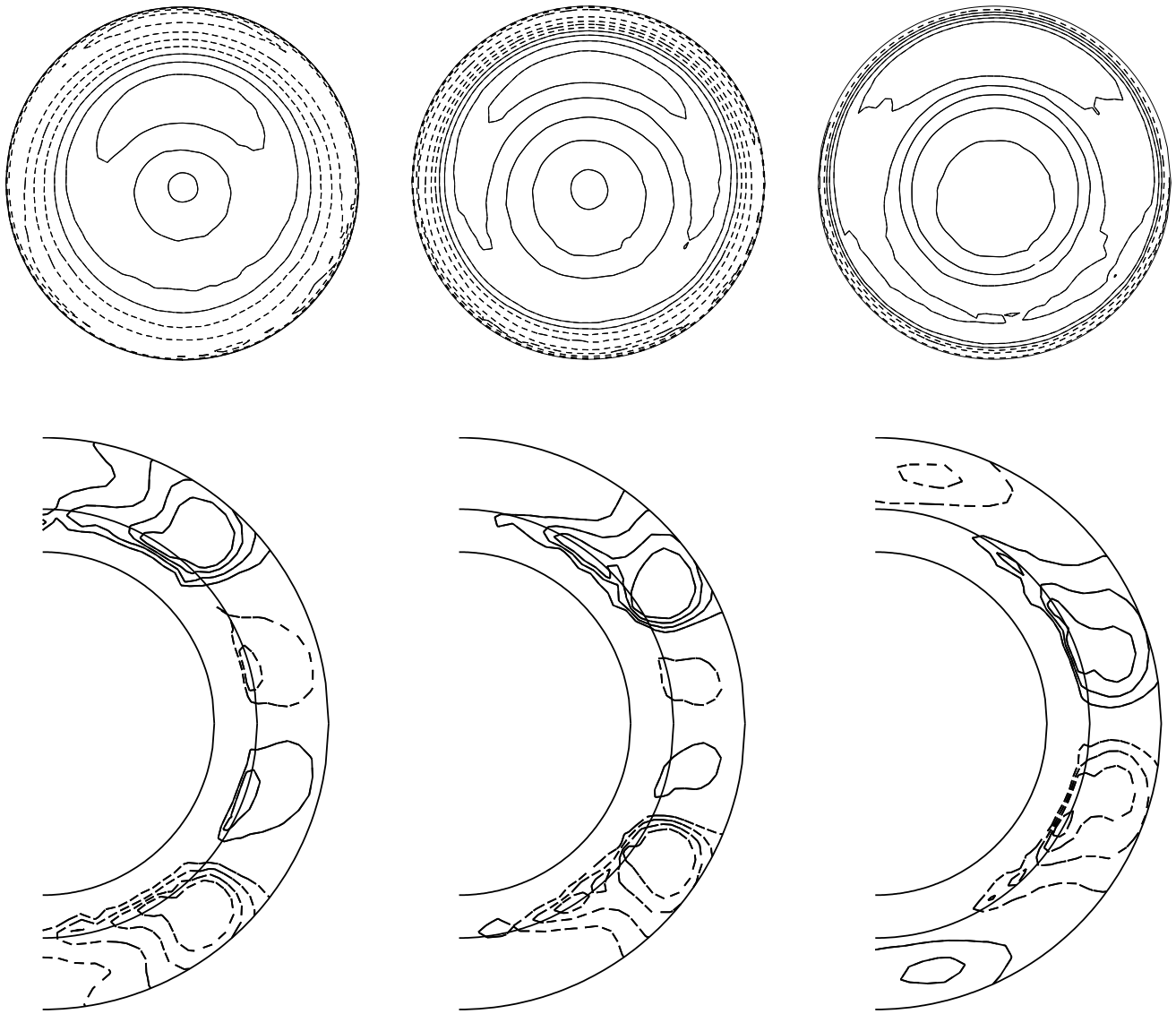

FIG. 9.—Contours of B_ϕ at the interface between the tachocline and convection zone, viewed from the South Pole (from top left to right), and contours of B_r in a meridional plane $\phi = \pi/2$ (from bottom left to right) for $\epsilon_\phi = 0.25$, $m = 1$, and $R_m = 200$ plotted at three different instants, $t = 4.2, 4.4, 4.6$. The contour levels for B_ϕ (B_r) are from -12 to 12 (-0.4 to 0.4).

meridional circulation may be critically important in the interface dynamo process since the site where the poloidal fields are produced remains a debated question. Our model follows the classical picture of Parker (1955) in that the α-effect is assumed to operate throughout the convection zone. Alternatively, an interface spherical dynamo may restrict the α-effect near the surface of the Sun (Babcock 1961), while the ω-effects still take place mainly in the tachocline. In this case, the two spatially separated magnetic field generation regions can be coupled by a single-cell meridional circulation having a poleward surface flow (Choudhuri et al. 1995; Dikpati & Charbonneau 1999; Küker et al. 2001). A large-scale circulation acts like a conveyer belt transporting magnetic fields between the tachocline and the solar surface. Dikpati & Gilman (2001b) also explored a different meridional flux transport dynamo in which the α-effects come from the global hydromagnetic or hydrodynamic instabilities taking place in the tachocline (Miesch 2001). It follows that the α-effects are independent of the flow turbulence in the convection zone but rely directly on instabilities, whether hydrodynamic or hydromagnetic or both, in the tachocline or on the decay of the active regions in the solar surface. To include those important effects in our fully three-dimensional model, extra terms are needed in equation (26) and several surface integrals are required in equation (36). The construction of a fully three-dimensional interface dynamo model that attempts to simulate the Sun and that includes the effects of the meridional circulation and the differential rotation, as well as the dynamical feedback of the Lorentz force, is currently underway.

K. Z. is supported by a UK NERC grant and would like to thank A. Gilbert for helpful discussions. J. Z. is supported by a UK NERC grant and by the HK RGC grant CUHK4292/00P. X. L. is supported by NSFC and MOST grants. G. S. is supported by grants from the NASA Planetary Geology and Geophysics and Planetary Atmospheres programs and from NSF under NSF EAR 00105945.

APPENDIX A

THE TOROIDAL FLOW THEOREM IN MULTISPHERICAL LAYERS

It was recognized by Bullard & Gellman (1954) that magnetic fields cannot be maintained by a purely differential rotation in a sphere. A comprehensive summary of the antidynamo theorems was given by Moffatt (1978). Here we extend the previous proof for a sphere to the spherical system of multiple layers with discontinuous magnetic diffusivities for the solar application.

Denote the magnetic field in the radiative core, the tachocline, the convection zone, and the exterior as $\boldsymbol{B}_i$, $\boldsymbol{B}_t$, $\boldsymbol{B}_o$, and $\boldsymbol{B}_e$, respectively. The simplest solar dynamo problem neglects both the meridional circulation $\boldsymbol{U}_P$ and turbulent convection (the α-effect) in the convection zone. The dynamo equation in each region within the Sun is then

$$\frac{\partial}{\partial t}\boldsymbol{B}_i(r,\theta,\phi,t) = \boldsymbol{\nabla}\times(\boldsymbol{\Omega}_c\times\boldsymbol{r})\times\boldsymbol{B}_i + \lambda_i\nabla^2\boldsymbol{B}_i\ , \qquad \text{in } V_i : 0 < r < r_i\ , \tag{A1}$$

$$\frac{\partial}{\partial t}\boldsymbol{B}_t(r,\theta,\phi,t) = \boldsymbol{\nabla}\times\{[f(r)\boldsymbol{\Omega}_T]\times\boldsymbol{r}\}\times\boldsymbol{B}_t + \lambda_t\nabla^2\boldsymbol{B}_t\ , \qquad \text{in } V_t : r_i < r < r_t\ , \tag{A2}$$

$$\frac{\partial}{\partial t}\boldsymbol{B}_o(r,\theta,\phi,t) = \boldsymbol{\nabla}\times(\boldsymbol{\Omega}_S\times\boldsymbol{r})\times\boldsymbol{B}_o + \lambda_o\nabla^2\boldsymbol{B}_o\ , \qquad \text{in } V_o : r_t < r < r_o\ , \tag{A3}$$

$$0 = \nabla^2\boldsymbol{B}_e\ , \qquad \text{in } V_e : r_o < r < \infty\ , \tag{A4}$$

where $\boldsymbol{\Omega}_c$ is the angular velocity of the whole radiative zone, $\boldsymbol{\Omega}_S(\theta)$ and $\boldsymbol{\Omega}_T(\theta)$ represent the differential rotation in the convection zone and the tachocline, respectively, and $f(r)$ is a function of the radius. We assume that $\boldsymbol{\Omega}_C$, $\boldsymbol{\Omega}_T$, and $\boldsymbol{\Omega}_S$ are continuous at the interfaces r_i and r_t. Different regimes are coupled by the magnetic matching conditions.

It is mathematically convenient to expand a general three-dimensional magnetic field, for example, $\boldsymbol{B}_t$ in the tachocline, in terms of the vector potentials g_t and h_t,

$$\boldsymbol{B}_t = \boldsymbol{\nabla}\times[\boldsymbol{r}g_t(r,\theta,\phi,t)] + \boldsymbol{\nabla}\times\boldsymbol{\nabla}\times[\boldsymbol{r}h_t(r,\theta,\phi,t)]\ , \tag{A5}$$

where

$$\boldsymbol{r}\cdot\boldsymbol{B}_t = \mathscr{L}h_t = -\left(\frac{1}{\sin\theta}\frac{\partial}{\partial\theta}\sin\theta\frac{\partial}{\partial\theta} + \frac{1}{\sin^2\theta}\frac{\partial}{\partial\phi^2}\right)h_t\ . \tag{A6}$$

The addition of any function $Y(r)$ to the scalar functions g_t and h_t has no effect on $\boldsymbol{B}_t$. Consequently, we can assume that g_t and h_t satisfy

$$\int_0^{2\pi}\left(\int_0^{\pi} g_t\sin\theta\,d\theta\right)d\phi = 0\ , \qquad \int_0^{2\pi}\left(\int_0^{\pi} h_t\sin\theta\,d\theta\right)d\phi = 0\ . \tag{A7}$$

The magnetic fields in other regions of the Sun can also be expanded in a similar way,

$$\boldsymbol{B}_i = \boldsymbol{\nabla}\times(\boldsymbol{r}g_i) + \boldsymbol{\nabla}\times\boldsymbol{\nabla}\times(\boldsymbol{r}h_i)\ ,$$

$$\boldsymbol{B}_c = \boldsymbol{\nabla}\times(\boldsymbol{r}g_o) + \boldsymbol{\nabla}\times\boldsymbol{\nabla}\times(\boldsymbol{r}h_o)\ ,$$

$$\boldsymbol{B}_e = \boldsymbol{\nabla}\times\boldsymbol{\nabla}\times(\boldsymbol{r}h_e)\ .$$

Here we have assumed that the exterior is vacuum and that $g_e = 0$ in V_e.

The equations for the poloidal field component can be obtained by forming the scalar product of the dynamo equation in each zone,

$$\frac{\partial}{\partial t}\mathscr{L}h_i + (\boldsymbol{\Omega}_c\times\boldsymbol{r})\cdot\boldsymbol{\nabla}\mathscr{L}h_i = (\boldsymbol{B}_i\cdot\boldsymbol{\nabla})[\boldsymbol{r}\cdot(\boldsymbol{\Omega}_c\times\boldsymbol{r})] + \lambda_i\nabla^2\mathscr{L}h_i\ , \tag{A8}$$

$$\frac{\partial}{\partial t}\mathscr{L}h_t + \{[f(r)\boldsymbol{\Omega}_T]\times\boldsymbol{r}\}\cdot\boldsymbol{\nabla}\mathscr{L}h_t = (\boldsymbol{B}_t\cdot\boldsymbol{\nabla})(\boldsymbol{r}\cdot\{[f(r)\boldsymbol{\Omega}_T]\times\boldsymbol{r}\}) + \lambda_t\nabla^2\mathscr{L}h_t\ , \tag{A9}$$

$$\frac{\partial}{\partial t}\mathscr{L}h_o + (\boldsymbol{\Omega}_S\times\boldsymbol{r})\cdot\boldsymbol{\nabla}\mathscr{L}h_o = (\boldsymbol{B}_o\cdot\boldsymbol{\nabla})[\boldsymbol{r}\cdot(\boldsymbol{\Omega}_S\times\boldsymbol{r})] + \lambda_o\nabla^2\mathscr{L}h_o\ , \tag{A10}$$

$$0 = \nabla^2\mathscr{L}h_e\ . \tag{A11}$$

The first term on the right-hand side of equations (A8)–(A10) vanishes. Multiplying, for example, the h_i equation by $\mathscr{L}h_i$ gives

$$\frac{\partial}{\partial t}\frac{1}{2\lambda_i}(\mathscr{L}h_i)^2 + \frac{1}{2\lambda_i}\boldsymbol{\nabla}\cdot[(\mathscr{L}h_i)^2(\boldsymbol{\Omega}_c\times\boldsymbol{r})] = \boldsymbol{\nabla}\cdot[(\mathscr{L}h_i)\boldsymbol{\nabla}(\mathscr{L}h_i)] - |\boldsymbol{\nabla}\mathscr{L}h_i|^2\ . \tag{A12}$$

Integration of equation (A12) over the radiative core V_i gives

$$\frac{\partial}{\partial t}\int_{V_i}\frac{1}{2\lambda_i}(\mathscr{L}h_i)^2 = -\int_{V_i}|\nabla\mathscr{L}h_i|^2 dV + \int_{\partial V_i}\left[(\mathscr{L}h_i)\frac{\mathscr{L}h_i}{\partial r}\right]dS\,, \tag{A13}$$

where ∂V_i denotes the interface between the core and the tachocline. By the same procedure, we can derive similar equations for other zones. The summation of all the equations obtained from different zones gives

$$\frac{\partial}{\partial t}\left[\int_{V_i}\frac{(\mathscr{L}h_i)^2}{2\lambda_i}dV + \int_{V_t}\frac{(\mathscr{L}h_t)^2}{2\lambda_t}dV + \int_{V_o}\frac{(\mathscr{L}h_o)^2}{2\lambda_o}dV\right] = -\left(\int_{V_i}|\nabla\mathscr{L}h_i|^2 dV + \int_{V_t}|\nabla\mathscr{L}h_t|^2 dV + \int_{V_o}|\nabla\mathscr{L}h_o|^2 dV + \int_{V_e}|\nabla\mathscr{L}h_e|^2 dV\right). \tag{A14}$$

All the boundary integrals are cancelled out by using the following boundary or matching conditions:

$$\begin{aligned}
\mathscr{L}h_i &= \mathscr{L}h_t\,, \qquad \frac{\partial\mathscr{L}h_i}{\partial r} = \frac{\partial\mathscr{L}h_t}{\partial r}\,, \qquad \text{at } r = r_i\,,\\
\mathscr{L}h_t &= \mathscr{L}h_o\,, \qquad \frac{\partial\mathscr{L}h_t}{\partial r} = \frac{\partial\mathscr{L}h_o}{\partial r}\,, \qquad \text{at } r = r_t\,,\\
\mathscr{L}h_o &= \mathscr{L}h_e\,, \qquad \frac{\partial\mathscr{L}h_o}{\partial r} = \frac{\partial\mathscr{L}h_e}{\partial r}\,, \qquad \text{at } r = r_o\,,\\
\mathscr{L}h_e &= O(r^{-2}) \to 0\,, \qquad \text{as } r \to \infty\,.
\end{aligned} \tag{A15}$$

It follows that the poloidal fields in all the zones starting with any initial condition must decay ultimately to zero with time.

Consider now the toroidal component of the magnetic field. In the radiative core, we have

$$\frac{\partial}{\partial t}\nabla\times(\boldsymbol{r}g_i) = \nabla\times[(\boldsymbol{\Omega}_c\times\boldsymbol{r})\times(\nabla\times\boldsymbol{r}g_i)] + \lambda\nabla^2[\nabla\times(\boldsymbol{r}g_i)]\,, \tag{A16}$$

which can be written as

$$\boldsymbol{r}\times\nabla\left[\frac{\partial g_i}{\partial t} + (\boldsymbol{\Omega}_c\times\boldsymbol{r})\cdot\nabla g_i - \lambda\nabla^2 g_i + F(r)\right] = 0\,, \tag{A17}$$

where $F(r)$ is an arbitrary function of r. In the following derivation, we use the identity

$$Q\nabla^2 Q = \nabla\cdot\left[\frac{Q}{r}\nabla(rQ)\right] - \left[\frac{1}{r}\hat{\boldsymbol{r}}\cdot\nabla(rQ)\right]^2 - |\nabla_H Q|^2\,,$$

where ∇_H is the gradient on a unit spherical surface

$$\nabla_H = \frac{\hat{\boldsymbol{\theta}}}{r}\frac{\partial}{\partial\theta} + \frac{\hat{\boldsymbol{\phi}}}{r\sin\theta}\frac{\partial}{\partial\phi}\,,$$

where $\hat{\boldsymbol{r}}, \hat{\boldsymbol{\theta}}, \hat{\boldsymbol{\phi}}$ are the unit vectors. We first uncurl equation (A17) and then multiply the resulting equation with g_i,

$$\frac{1}{2}\frac{\partial g_i^2}{\partial t} + \frac{1}{2}\nabla\cdot\left[g_i^2(\boldsymbol{\Omega}\times\boldsymbol{r})\right] = \lambda_i\left\{\nabla\cdot\left[\frac{g_i}{r}\nabla(rg_i)\right] - \left[\frac{1}{r}\hat{\boldsymbol{r}}\cdot\nabla(rg_i)\right]^2 - |\nabla_H g_i|^2 + g_i F(r)\right\}. \tag{A18}$$

Integration of equation (A18) over the radiative core in V_i gives

$$\frac{1}{2}\frac{\partial}{\partial t}\int_V g_i^2\,dV = \int_{\partial V_i}\lambda_i\left(\frac{g_i}{r}\hat{\boldsymbol{r}}\cdot\nabla(rg_i)\right)dS - \lambda_i\int_{V_i}\left\{\left[\frac{1}{r}\hat{\boldsymbol{r}}\cdot\nabla(rg_i)\right]^2 + |\nabla_H g_i|^2\right\}dV\,. \tag{A19}$$

Summing all the similar equations obtained from different zones gives

$$\begin{aligned}
\frac{1}{2}\frac{\partial}{\partial t}\left(\int_{V_i} g_i^2\,dV + \int_{V_t} g_t^2\,dV + \int_{V_o} g_o^2\,dV\right) = &-\lambda_i\int_{V_i}\left\{\left[\frac{1}{r}\hat{\boldsymbol{r}}\cdot\nabla(rg_i)\right]^2 + |\nabla_H g_i|^2\right\}dV - \lambda_t\int_{V_t}\left\{\left[\frac{1}{r}\hat{\boldsymbol{r}}\cdot\nabla(rg_t)\right]^2 + |\nabla_H g_t|^2\right\}dV\\
&-\lambda_o\int_{V_o}\left\{\left[\frac{1}{r}\hat{\boldsymbol{r}}\cdot\nabla(rg_o)\right]^2 + |\nabla_H g_o|^2\right\}dV\,.
\end{aligned} \tag{A20}$$

Here we have made use of the matching or boundary conditions that the magnetic field and tangential electric field must be

continuous:

$$\begin{aligned} &g_i = g_t\ , && \lambda_i \hat{\boldsymbol{r}} \cdot \boldsymbol{\nabla}(r g_i) = \lambda_t \hat{\boldsymbol{r}} \cdot \boldsymbol{\nabla}(r g_t) && \text{at } r = r_i\ , \\ &g_t = g_o\ , && \lambda_t \hat{\boldsymbol{r}} \cdot \boldsymbol{\nabla}(r g_t) = \lambda_o \hat{\boldsymbol{r}} \cdot \boldsymbol{\nabla}(r g_o) && \text{at } r = r_t\ , \\ &g_o = 0\ , && && \text{at } r = r_o\ . \end{aligned} \tag{A21}$$

The last condition is related to the vacuum boundary condition. As a result, the integrals of g_i^2, g_t^2, and g_o^2 vanish as $t \to \infty$, so that

$$g_i = g_t = g_o = 0\ .$$

The conclusion is that any profile of purely differential rotation in the Sun with a radially discontinuous profile of the magnetic diffusivities cannot sustain the solar magnetic field.

APPENDIX B

COWLING'S THEOREM IN MULTISPHERICAL LAYERS

After the solar dynamo proposal first put forward by Larmor (1919), it was Cowling (1934) who proved that a steady axisymmetric poloidal field cannot be maintained by dynamo processes. Cowling's theorem was later extended to the more general case that any axisymmetric magnetic field in a sphere cannot be self-sustained (Braginsky 1964; see also Moffatt 1978). In this appendix we prove that the combination of differential rotation $\boldsymbol{\Omega}(r, \theta)$ and meridional circulation $\boldsymbol{U}_p(r, \theta)$ with a radially discontinuous profile of the magnetic diffusivity cannot produce a self-exciting axisymmetric dynamo in the Sun.

An axisymmetric magnetic field in the different zones is governed by

$$\frac{\partial}{\partial t}\boldsymbol{B}_i(r, \theta, t) = \boldsymbol{\nabla} \times [(\boldsymbol{\Omega}_c \times \boldsymbol{r}) \times \boldsymbol{B}_i] + \lambda_i \nabla^2 \boldsymbol{B}_i\ , \qquad \text{in } V_i : 0 \le r < r_i\ , \tag{B1}$$

$$\frac{\partial}{\partial t}\boldsymbol{B}_t(r, \theta, t) = \boldsymbol{\nabla} \times \{[f(r)\boldsymbol{\Omega}_T \times \boldsymbol{r}] \times \boldsymbol{B}_t\} + \lambda_t \nabla^2 \boldsymbol{B}_t\ , \qquad \text{in } V_t : r_i < r < r_t\ , \tag{B2}$$

$$\frac{\partial}{\partial t}\boldsymbol{B}_o(r, \theta, t) = \boldsymbol{\nabla} \times \{[(\boldsymbol{\Omega}_S \times \boldsymbol{r}) + \boldsymbol{U}_p] \times \boldsymbol{B}_o\} + \lambda_o \nabla^2 \boldsymbol{B}_o\ , \qquad \text{in } V_o : r_t < r < r_o\ , \tag{B3}$$

$$0 = \nabla^2 \boldsymbol{B}_e\ , \qquad \text{in } V_e : r_o < r < \infty\ . \tag{B4}$$

For the purpose of mathematical proof, we can express the axisymmetric field using the poloidal and toroidal flux functions $\Phi(r, \theta, t)$ and $\Psi(r, \theta, t)$, respectively, for example,

$$\boldsymbol{B}_o = \boldsymbol{\nabla} \times \left[\left(\frac{\Phi_o}{r \sin\theta}\right)\hat{\boldsymbol{\phi}}\right] + (r \sin\theta \Psi_o)\hat{\boldsymbol{\phi}}\ ,$$

which satisfies the solenoidal condition automatically.

First, we look at the poloidal component of the dynamo equation, for example, in the convection zone,

$$\boldsymbol{\nabla} \times \left\{\frac{\partial}{\partial t}\left[\left(\frac{\Phi_o}{r \sin\theta}\right)\hat{\boldsymbol{\phi}}\right] + \left(\frac{1}{r \sin\theta}\boldsymbol{U}_P \cdot \boldsymbol{\nabla}\Phi_o\right)\hat{\boldsymbol{\phi}} - \lambda_o \mathscr{D}^2\left(\frac{\Phi_o}{r \sin\theta}\right)\hat{\boldsymbol{\phi}} + \boldsymbol{\nabla}F(r, \theta)\right\} = 0\ , \tag{B5}$$

where

$$\mathscr{D}^2\left(\frac{\Phi_o}{r \sin\theta}\right) = \frac{1}{r \sin\theta}\left[\nabla^2 \Phi_o - \frac{2}{r \sin\theta}\boldsymbol{\nabla}(r \sin\theta) \cdot \boldsymbol{\nabla}\Phi_o\right]\ .$$

We first uncurl equation (B5) and form the scalar product of the ϕ-component of the equation with $\hat{\boldsymbol{\phi}}$. We then multiply the resulting equation by Φ_o,

$$\frac{1}{2\lambda_o}\left[\frac{\partial}{\partial t}\Phi_o^2 + \boldsymbol{\nabla} \cdot \left(\Phi_o^2 \boldsymbol{U}_P\right)\right] = \boldsymbol{\nabla} \cdot (\Phi_o \boldsymbol{\nabla}\Phi_o) - |\boldsymbol{\nabla}\Phi_o|^2 - \boldsymbol{\nabla} \cdot \left\{\left[\frac{(\sin\theta)\hat{\boldsymbol{r}} + (\cos\theta)\hat{\boldsymbol{\theta}}}{r \sin\theta}\right]\Phi_o^2\right\}\ . \tag{B6}$$

Integration of equation (B6) over the convection zone V_o and use of the velocity boundary condition $\hat{\boldsymbol{r}} \cdot \boldsymbol{U}_P = 0$ give

$$\frac{\partial}{\partial t}\left(\int_{V_o}\frac{1}{2\lambda_o}\Phi_o^2\, dV\right) = -\int_{V_o}|\boldsymbol{\nabla}\Phi_o|^2 dV + \left(\int_{\partial V_o} - \int_{\partial V_t}\right)\left[\Phi_o \frac{\partial \Phi_o}{\partial r} - \frac{\Phi_o^2}{r}\right] dS\ , \tag{B7}$$

where ∂V_t and ∂V_o denote spherical surfaces at $r = r_t$ and $r = r_o$. By the same procedure we can derive similar equations for

other zones in the Sun. The summation of these equations gives

$$\frac{\partial}{\partial t}\left(\int_{V_i}\frac{\Phi_i^2}{2\lambda_i}dV+\int_{V_t}\frac{\Phi_t^2}{2\lambda_t}dV+\int_{V_o}\frac{\Phi_o^2}{2\lambda_o}dV\right)=-\left(\int_{V_i}|\nabla\Phi_i|^2dV+\int_{V_t}|\nabla\Phi_t|^2dV+\int_{V_o}|\nabla\Phi_o|^2dV+\int_{V_e}|\nabla\Phi_e|^2dV\right). \quad \text{(B8)}$$

All the boundary integrals at the various interfaces either are cancelled out or vanish by using the matching or boundary conditions,

$$\begin{aligned}
&\Phi_i=\Phi_t\,, \quad \frac{\partial\Phi_i}{\partial r}=\frac{\partial\Phi_t}{\partial r}\,, && \text{at } r=r_i\,,\\
&\Phi_t=\Phi_o\,, \quad \frac{\partial\Phi_t}{\partial r}=\frac{\partial\Phi_o}{\partial r}\,, && \text{at } r=r_t\,,\\
&\Phi_o=\Phi_e\,, \quad \frac{\partial\Phi_o}{\partial r}=\frac{\partial\Phi_e}{\partial r}\,, && \text{at } r=r_o\,,\\
&\Phi_e=O\left(r^{-1}\right)\rightarrow 0\,, && \text{as } r\rightarrow\infty\,.
\end{aligned} \quad \text{(B9)}$$

Equation (B8) implies that the poloidal fields in all the zones starting with any initial condition must decay ultimately to zero with time.

The equation for the toroidal component of magnetic field can be obtained by the ϕ-component of the dynamo equation, for example, in the convection zone,

$$\frac{\partial\Psi_o}{\partial t}+\boldsymbol{U}_P\cdot\nabla\Psi_o=\left\{\nabla\times\left[\left(\frac{\Phi_o}{r\sin\theta}\right)\hat{\boldsymbol{\phi}}\right]\right\}\cdot\nabla|\boldsymbol{\Omega}_S|+\frac{\lambda_o}{r\sin\theta}\hat{\boldsymbol{\phi}}\cdot\nabla^2\left(r\sin\theta\Psi_o\hat{\boldsymbol{\phi}}\right). \quad \text{(B10)}$$

It is crucial that the poloidal magnetic field $\Phi_0\rightarrow 0$, as suggested by equation (B8). In consequence, there is no source term for the toroidal flux Ψ_o. Multiplication of equation (B10) with Ψ_o and use of the identity

$$\frac{Q}{r\sin\theta}\hat{\boldsymbol{\phi}}\cdot\nabla^2\left(r\sin\theta Q\hat{\boldsymbol{\phi}}\right)=\nabla\cdot\left[\frac{Q}{r}\nabla(rQ)\right]-|\nabla Q|^2+\nabla\cdot\left[\left(\frac{Q^2\cot\theta}{r}\right)\hat{\boldsymbol{\theta}}\right]$$

give

$$\frac{1}{2}\frac{\partial\Psi_o^2}{\partial t}+\frac{1}{2}\nabla\cdot\left(\boldsymbol{U}_P\Psi_o^2\right)=\lambda_o\left\{\nabla\cdot\left[\frac{\Psi_o}{r}\nabla(r\Psi_o)\right]-|\nabla\Psi_o|^2+\nabla\cdot\left[\left(\frac{\Psi_o^2\cot\theta}{r}\right)\hat{\boldsymbol{\theta}}\right]\right\}. \quad \text{(B11)}$$

Integration of the equation over the convection zone in V_o gives

$$\frac{1}{2}\frac{\partial}{\partial t}\int_{V_o}\Psi_o^2\,dV=-\lambda_o\int_{V_o}|\nabla\Psi_o|^2dV+\left(\int_{\partial V_t}-\int_{\partial V_o}\right)\frac{1}{r}[\lambda_o\Psi_o\hat{\boldsymbol{r}}\cdot\nabla(r\Psi_o)]dS\,. \quad \text{(B12)}$$

The summation of the integral equations obtained from different zones cancels out all the surface integrals, giving rise to

$$\frac{1}{2}\frac{\partial}{\partial t}\left(\int_{V_i}\Psi_i^2\,dV+\int_{V_t}\Psi_t^2\,dV+\int_{V_o}\Psi_o^2\,dV\right)=-\left[\lambda_i\int_{V_i}|\nabla\Psi_i|^2dV+\lambda_t\int_{V_t}|\nabla\Psi_t|^2dV+\lambda_o\int_{V_o}|\nabla\Psi_o|^2dV\right]. \quad \text{(B13)}$$

In the derivation, we have used the following matching or boundary conditions:

$$\begin{aligned}
&\Psi_i=\Psi_t\,, \quad \lambda_i\hat{\boldsymbol{r}}\cdot\nabla(r\Psi_i)=\lambda_t\hat{\boldsymbol{r}}\cdot\nabla(r\Psi_t)\,, && \text{at } r=r_i\,,\\
&\Psi_t=\Psi_o\,, \quad \lambda_t\hat{\boldsymbol{r}}\cdot\nabla(r\Psi_t)=\lambda_o\hat{\boldsymbol{r}}\cdot\nabla(r\Psi_o)\,, && \text{at } r=r_t\,,\\
&\Psi_o=0\,, && \text{at } r=r_o\,.
\end{aligned} \quad \text{(B14)}$$

It follows that the integrals of Ψ_i^2, Ψ_t^2, and Ψ_o^2 vanish as $t\rightarrow\infty$, so that

$$\Psi_i=\Psi_t=\Psi_o=0\,.$$

In the Sun's interior characterized by a radially discontinuous variation of the magnetic diffusivity, any combination of differential rotation $\boldsymbol{\Omega}(r,\theta)$ and meridional circulation $\boldsymbol{U}_P$ cannot sustain an axisymmetric solar magnetic field. These anti-dynamo theories make the α-effect in equation (15) a critically important ingredient in an interface dynamo, although the nature of the dynamo is largely determined by the strong shear flow in the tachocline.

REFERENCES

Babcock, H. W. 1961, ApJ, 133, 572
Braginsky, S. I. 1964, Soviet Phys.—JETP Lett., 20, 726
Brandenburg, A. 1994, in Lectures on Solar and Planetary Dynamos, ed. M. R. E. Proctor & A. D. Gilbert (Cambridge: Cambridge Univ. Press), 117
Brandenburg, A., Krause, F., Meinel, R., Moss, D., & Tuominen, I. 1989, A&A, 213, 411
Brown, T. M., et al. 1989, ApJ, 343, 526
Bullard, E. C., & Gellman, H. 1954, Philos. Trans. R. Soc. London, A247, 213

Caligari, P., Moreno-Insertis, F., & Schussler, M. 1995, ApJ, 441, 886
Cally, P. S. 2001, Sol. Phys., 199, 231
Chan, K. H., Zhang, K., Zou, J., & Schubert, G. 2001, Phys. Earth Planet. Inter., 128, 35
Charbonneau, P., & MacGregor, K. B. 1997, ApJ, 486, 502
Choudhuri, A. R., Schüssler, M., & Dikpati, M. 1995, A&A, 303, L29
Cowling, T. G. 1934, MNRAS, 94, 39
Dikpati, M., & Charbonneau, P. 1999, ApJ, 518, 508
Dikpati, M., & Gilman, P. A. 2001a, ApJ, 551, 536
———. 2001b, ApJ, 559, 428
Fan, Y., Fisher, G. H., & De Luca, E. E. 1993, ApJ, 405, 390
Gilman, P. A., & Dikpati, M. 2002, ApJ, 576, 1031
Gilman, P. A., & Fox, P. A. 1997, ApJ, 484, 439
Glatzmaier, G. A., & Gilman, P. 1982, ApJ, 256, 316
Gough, D. O., Leibacher, J. W., Scherrer, P. H., & Toomre, J. 1996, Science, 272, 1281
Gough, D. O., & McIntyre, M. E. 1998, Nature, 394, 755
Gubbins, D., Barber, C. N., Gibbons, S., & Love, J. J. 2000, Proc. R. Soc. London A, 456, 1333
Hollerbach, R., & Jones, C. A. 1993, Nature, 365, 541
Kosovichev, A. G. 1996, ApJ, 469, L61
Küker, M., Rüdiger, G., & Schultz, M. 2001, A&A, 374, 301
Larmor, J. 1919, Rep. Brit. Assn. Adv. Sci. 159
MacGregor, K. B., & Charbonneau, P. 1997, ApJ, 486, 484
Markiel, J. A., & Thomas, J. H. 1999, ApJ, 523, 827
Miesch, M. S. 2001, ApJ, 562, 1058
Moffatt, H. K. 1978, Magnetic Field Generation in Electrically Conducting Fluids (Cambridge: Cambridge Univ. Press)
Moss, D., & Brandenburg, A. 1995, Geophys. Astrophys. Fluid Dyn., 80, 229
Moss, D., Tuominen, I., & Brandenburg A. 1991, A&A, 245, 129
Parker, E. N. 1955, ApJ, 122, 293
———. 1970, ApJ, 160, 383
———. 1993, ApJ, 408, 707
Ponty, Y., Gilbert, A., & Soward, A. M. 2001, J. Fluid Mech., 435, 261
Roberts, P., & Stix, M. 1972, A&A, 18, 453
Roberts, P. H. 1972, Philos. Trans. R. Soc. London, A272, 663
Rüdiger, G. 1980, Astron. Nachr., 301, 181
Schou, J. 1991, in Proc. Conf. at Inst. Theor. Phys., ed. D. Gough & R. Toomre (Berlin: Springer), 81
Schou, J., et al. 1998, ApJ, 505, 390
Schubert, G., & Zhang, K. 2000, ApJ, 532, L149
Spiegel, E. A., & Zahn, J.-P. 1992, A&A, 265, 106
Stix, M. 1989, The Sun: An Introduction (Berlin: Springer)
Tobias, S. M. 1997, A&A, 322, 1007
Tobias, S. M., Weiss, N. O., & Kirk, V. 1995, MNRAS, 273, 1150
Weiss, N. O. 1994, in Lectures on Solar and Planetary Dynamos, ed. M. R. E. Proctor & A. D. Gilbert (Cambridge: Cambridge Univ. Press), 59
Zhang, K., & Busse, F. 1989, Geophys. Astrophys. Fluid Dyn., 49, 97
Zhang, K., Liao, X., & Schubert, G. 2003, ApJ, 585, 1124